

# A finite particle method (FPM) for Lagrangian simulation of conservative solute transport in heterogeneous porous media

Tian Jiao <sup>a,b</sup>, Ming Ye <sup>b,\*</sup>, Menggui Jin <sup>a,\*</sup>, Jing Yang <sup>a,b</sup>

<sup>a</sup> School of Environmental Studies, China University of Geosciences, Wuhan 430074, China

<sup>b</sup> Department of Earth, Ocean, and Atmosphere Science and Department of Scientific Computing, Florida State University, Tallahassee, FL 32306, USA



## ARTICLE INFO

### Keywords:

Advection-dispersion equation  
Finite particle method (FPM)  
Smoothed particle hydrodynamic  
Particle irregularity  
Heterogeneous flow field

## ABSTRACT

When a smoothed particle hydrodynamics (SPH) method, a Lagrangian and meshfree numerical scheme, is used to solve the advection-dispersion equation (ADE), SPH solutions may not be accurate when particles are irregularly distributed, i.e., the distance between two neighbor particles varies irregularly in a simulation domain. Particle irregularity may be caused by nonuniform groundwater flow in a heterogeneous field of hydraulic conductivity. This study explores for the first time whether the Finite Particle Method (FPM) can provide more accurate ADE solutions than SPH does for irregularly distributed particles. FPM is similar to SPH in theory, but uses a modified kernel gradient to construct a SPH approximation of solute concentration gradients. Performance of SPH and FPM with irregularly distributed particles is evaluated by using two numerical cases. The first case considers only diffusive transport, and has an analytical solution for the evaluation. The second case considers both advection and dispersion, and uses a numerical solution as a reference for the evaluation. For each of the two cases, several numerical experiments are conducted using multiple sets of irregularly distributed particles with different levels of particle irregularity due to different levels of heterogeneity of hydraulic conductivity. Numerical results indicate that, for the numerical experiments of this study, FPM outperforms SPH to yield more accurate ADE solutions. However, FPM solutions are still subject to numerical errors, and the errors increase when the level of heterogeneity of hydraulic conductivity increases. Further improvement of FPM is warranted in a future study.

## 1. Introduction

While considerable advancements have been made for numerically solving the advection-dispersion equation (ADE) in porous media, there are still a number of open questions to obtain accurate numerical solutions of solute transport in a heterogeneous aquifer with non-uniform velocity (Boso et al., 2013; de Barros et al., 2015; Herrera et al., 2017; Konikow, 2011; Radu et al., 2011; Werth et al., 2006; Sole-Mari and Fernández-García, 2018; Zhou et al., 2020; Radu et al., 2011). One of the questions is the numerical dispersion that overestimates solute mixing, which occurs often in traditional grid-based methods such as finite difference and finite element methods (Radu et al., 2011; Zheng and Wang, 1999). Different from the grid-based methods, Lagrangian approaches theoretically can eliminate numerical dispersion by handling the ADE's advection term using particle tracking approaches. One of the Lagrangian approaches is the smoothed particle hydrodynamics (SPH) method that uses particle movement to take account of the advection

term (e.g., Tartakovsky et al., 2007a,b, 2009; Herrera et al., 2009, 2010, 2017; de Barros et al., 2015; Benson et al., 2017; Avesani et al., 2017; Zhu and Fox 2001; Alvarado-Rodríguez et al., 2019). Boso et al. (2013) compared SPH with four grid-based and Lagrangian methods for simulating nonreactive and reactive solute transport in heterogeneous porous media, and showed the potential of SPH to reduce the impacts of numerical dispersion on ADE numerical solutions. However, Herrera and Beckie (2013) found that standard SPH methods are highly sensitive to spatial distributions of particles, and that SPH simulation accuracy is heavily influenced by the particle irregularity problem discussed in detail by Monaghan (2005).

When using SPH to solve the ADE, the ADE's dispersion term is approximated by a kernel integral interpolation over a support domain, and accuracy of the approximation depends on spatial distribution of the particles used in SPH (Liu and Liu, 2010; Monaghan, 2005). The particle spatial distribution in turn depends on groundwater flow fields. If groundwater seepage velocity's magnitude and direction are constant

\* Corresponding authors.

E-mail addresses: [tianjiao@cug.edu.cn](mailto:tianjiao@cug.edu.cn) (T. Jiao), [mye@fsu.edu](mailto:mye@fsu.edu) (M. Ye), [mgjin@cug.edu.cn](mailto:mgjin@cug.edu.cn) (M. Jin), [jingyang@cug.edu.cn](mailto:jingyang@cug.edu.cn) (J. Yang).

over a model domain, when the particles move with groundwater flow, the relative particle positions do not change over space. If the particles are uniformly distributed in space (i.e., the distance between two particles is a constant over the model domain), accurate SPH solutions can be obtained. For a groundwater flow in a heterogeneous field of hydraulic conductivity, groundwater seepage velocity's magnitude and direction vary in space and time. This leads to more particles in locations where pathlines converge and less particles in space where the pathlines diverge. In other words, particles are irregularly distributed in space, and such an irregular particle distribution may cause large numerical errors in SPH-based ADE solutions (Tartakovsky, 2010). When simulation time increases, the particle distribution becomes more irregular, and the corresponding numerical errors cumulate over time to cause significant numerical errors and instability.

Several methods have been developed to improve SPH for irregular particle distributions. One method uses a remeshing technique to periodically remesh irregularly distributed particles on a uniform grid and to interpolate particle properties (e.g., solute concentration) to new particle locations (Zimmermann, 2001; Chaniotis et al., 2003). Avesani et al. (2015) developed a modified SPH method based on the Moving-Least-Squares-Weighted-Essentially-Non-Oscillatory (MLS-WENO) reconstruction of concentrations. The method applies MLS-WENO to moving particles for accurate reproduction of concentration gradients. Avesani et al. (2015) showed that, in comparison with a standard SPH method, the modified SPH method is less sensitive to particle spatial distributions due to a better estimation of spatially varying concentration fluxes. However, the modified SPH method is computationally expensive due to intermediate steps involved in MLS-WENO reconstruction of concentrations. When using comparable particle spacings and support domains, the modified SPH method requires up to two orders of magnitude more CPU time than a standard SPH does. Although the computational time of the modified SPH can be reduced by using the ADER-WENO-SPH method developed by Avesani et al. (2021), where ADER stands for Arbitrary DERivatives, ADER-WENO-SPH has not been applied to groundwater solute transport problems. Alvarado-Rodríguez et al. (2019) presented a consistent SPH method, which resolves the particle irregularity problem by adjusting the number of neighbor particles in a support domain based on the relation between the support domain size and the number of particles derived by Zhu et al. (2015) and Sigalotti et al. (2016). Using a large number of neighbor particles requires a large amount of computational memory. In addition, adjusting the number of neighbor particles is not straightforward because the degree of particle irregularity changes in space and time.

This study is focused on the Finite Particle Method (FPM) that was developed by Liu et al. (2005, 2006) based on the corrective SPH method of Chen et al. (1999) and Chen and Beraun (2000). FPM constructs improved SPH approximations of a function and the function's derivatives (the function can be solute concentrations in the context of solving ADE). FPM is in theory similar to the modified SPH method developed by Zhang and Batra (2004) and Batra and Zhang (2004) in the field of solid mechanics. In the field of computational fluid dynamics, Xu and Deng (2016) used FPM to model transient free-surface flows of viscous and viscoelastic fluids, and Zhang et al. (2019) coupled FPM with a particle shifting technique to model particulate flows with thermal convection. Other applications of FPM can be found in Huang et al. (2018), Montanino et al. (2017), Zhang and Batra (2008), and Zhang et al. (2018).

FPM has not been used for solving ADE, and this study is the first attempt in the groundwater modeling community to explore whether FPM can resolve the problem of irregularly distributed particles for solving groundwater flow and solute transport in heterogeneous porous media. The irregular particle distributions considered in this study are caused by nonuniform groundwater due to heterogeneous hydraulic conductivity, and the distance between two neighbor particles is irregular. When the distance is constant over a simulation domain, the

corresponding particle distribution is called a uniform particle distribution. We demonstrate from a theoretical perspective that SPH approximations are accurate for uniform particle distributions, but may not be the case for irregular particle distributions. FPM improves SPH by using a modified kernel gradient to construct the SPH approximation of concentration gradients. The performance of FPM for solving ADE in heterogeneous flow fields with irregularly distributed particles is evaluated by using two numerical cases. The first case considers only diffusive transport, and has an analytical solution that can be used to evaluate accuracy of SPH and FPM solutions. The second case considers both advection and dispersion, and uses a numerical solution as a reference to evaluate accuracy of SPH and FPM solutions. For each of the two cases, several numerical experiments are conducted using multiple irregularly distributed particles with different levels of particle irregularity.

## 2. Mathematical model and numerical schemes

The ADE is given as

$$\frac{\partial C}{\partial t} + \mathbf{v} \cdot \nabla C = \nabla \cdot (\mathbf{D} \nabla C) \quad (1)$$

where  $C$  is the solute concentration,  $\mathbf{D}$  is a tensor of dispersion coefficient, and  $\mathbf{v}$  is a vector of seepage velocity. In Lagrangian coordinates, this equation is written as (Herrera et al., 2009):

$$\frac{d\mathbf{x}}{dt} = \mathbf{v} \quad (2)$$

$$\frac{dC}{dt} = \nabla \cdot (\mathbf{D} \nabla C) \quad (3)$$

where  $\mathbf{x}$  is the position of a particle. The substantial derivative,  $dC/dt = \partial C/\partial t + \mathbf{v} \partial C/\partial \mathbf{x}$ , represents time rate change of solute concentration along the pathline of a particle.

### 2.1. Smoothed particle hydrodynamics and particle irregularity problems

In SPH, Eqs. (2) and (3) are approximated by using a finite number of particles to carry the solute concentration. Eq. (2) governs movement of the particles, and Eq. (3) defines the diffusive transport component. The solution of Eq. (3) for the particles is evaluated using a kernel interpolation approximation. The approximations of concentration  $C(\mathbf{x})$  and its spatial derivative,  $\nabla C(\mathbf{x})$ , at position  $\mathbf{x}$  are written as (Liu and Liu, 2010)

$$\langle C(\mathbf{x}) \rangle = \int_{\Omega} C(\mathbf{x}') W(\mathbf{x} - \mathbf{x}', h) d\mathbf{x}' \quad (4)$$

$$\langle \nabla C(\mathbf{x}) \rangle = - \int_{\Omega} C(\mathbf{x}') \nabla W(\mathbf{x} - \mathbf{x}', h) d\mathbf{x}' \quad (5)$$

where  $\langle \rangle$  denotes the approximations,  $W$  is a kernel function,  $h$  is the smoothing length that defines a support domain of the kernel function,  $\mathbf{x}'$  is the location of a neighbor particle of the particle at  $\mathbf{x}$  within the support domain,  $\Omega$  is the support domain whose radius is in general several times of  $h$ , and the gradient,  $\nabla W(\mathbf{x} - \mathbf{x}', h) = \nabla W(\mathbf{x} - \mathbf{x}', h)|_{\mathbf{x}'}$ , of  $W$  is evaluated at  $\mathbf{x}'$ . Information of all the particles inside the support domain is used to determine the information of the particle at  $\mathbf{x}$  (Liu and Liu, 2003). According to Liu and Liu (2010), the kernel function  $W$  should be sufficiently smooth, and satisfies the following properties:

- (1) Positive property,  $W(\mathbf{x} - \mathbf{x}') \geq 0$ ,
- (2) Unity property,  $\int_{\Omega} W(\mathbf{x} - \mathbf{x}', h) d\mathbf{x}' = 1$ ,
- (3) Symmetric property,  $\int_{\Omega} (\mathbf{x}' - \mathbf{x}) W(\mathbf{x} - \mathbf{x}', h) d\mathbf{x}' = 0$ ,
- (4) Delta function property,  $\lim_{h \rightarrow 0} W(\mathbf{x} - \mathbf{x}', h) = \delta(\mathbf{x} - \mathbf{x}')$ ,
- (5) Compact condition,  $W(\mathbf{x} - \mathbf{x}') = 0$ , for  $|\mathbf{x} - \mathbf{x}'| > kh$  with  $k$  being an integer, and

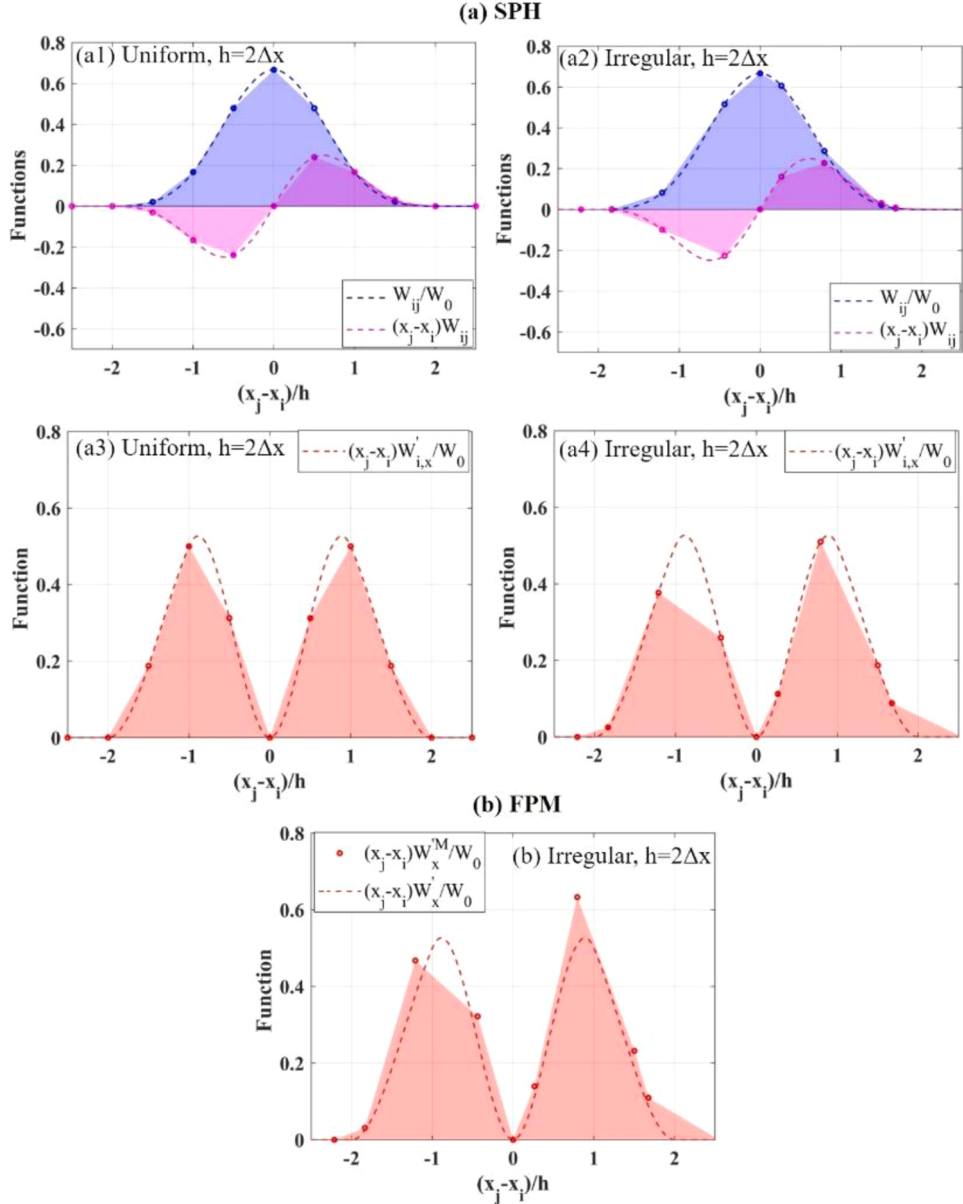


**Fig. 1.** (a1-a2) Illustration of the unity and symmetric properties of a SPH kernel function for uniformly and irregularly distributed particles in a one-dimensional domain. (a3-a4) Illustration of the anti-symmetric property of the SPH kernel function's gradient for uniformly and irregularly distributed particles in a one-dimensional domain. (b) Illustration of the anti-symmetric property using the modified kernel gradient based on the same SPH kernel function.

(6) Monotonical property that  $W$  monotonically decreases with  $h$ .

For illustrative purpose, the commonly used cubic B-spline function is chosen as the kernel function (Monaghan, 2005) in this study,

$$W = W_0 \times \begin{cases} 2/3 - q^2 + q^3/2 & 0 \leq q < 1 \\ (2-q)^3/6 & 1 \leq q < 2 \\ 0 & q \geq 2, \end{cases} \quad (6)$$

where  $q = |\mathbf{x} - \mathbf{x}'|/h$  is the relative distance between two particles at locations  $\mathbf{x}$  and  $\mathbf{x}'$ ,  $W_0$  is a normalization factor with  $W_0 = 1/h$  for a one-dimensional space,  $W_0 = 15/(7\pi h^2)$  for a two-dimensional space and  $W_0 = 3/(2\pi h^3)$  for a three-dimensional space. Other kernel functions (e.g., Gaussian function and Wendland function) (Dehnen and Aly, 2012) can also be used for FPM, and the discussion and conclusions of this study based on the cubic B-spline function are expected to be valid for other kernel functions.

The integrals in Eqs. (4) and (5) around particle  $i$  at position  $\mathbf{x}_i$  within

the support domain can be approximated as a summation over all neighbor particles  $j$  at position  $\mathbf{x}_j$ . These approximations are called particle approximations, and they are

$$\langle C(\mathbf{x}_i) \rangle = \langle C_i \rangle = \int_{\Omega} C(\mathbf{x}') W(\mathbf{x} - \mathbf{x}', h) d\mathbf{x}' = \sum_{j=1}^{N_b} \frac{m_j}{\rho_j} C(\mathbf{x}_j) W_{ij} = \sum_{j=1}^{N_b} \frac{m_j}{\rho_j} C_j W_{ij} \quad (7)$$

$$\begin{aligned} \langle \nabla C(\mathbf{x}_i) \rangle &= \langle \nabla C_i \rangle = - \int_{\Omega} C(\mathbf{x}') \nabla W(\mathbf{x} - \mathbf{x}', h) d\mathbf{x}' \\ &= - \sum_{j=1}^{N_b} \frac{m_j}{\rho_j} C(\mathbf{x}_j) \nabla_j W_{ij} = \sum_{j=1}^{N_b} \frac{m_j}{\rho_j} C_j \nabla_j W_{ij} \end{aligned} \quad (8)$$

where  $C_i = C(\mathbf{x}_i)$ ,  $C_j = C(\mathbf{x}_j)$ ,  $N_b$  is the number of particles within the support domain of particle  $i$ ,  $W_{ij} = W(|\mathbf{x}_i - \mathbf{x}_j|, h)$ ,  $\nabla_j W_{ij}$  is the gradient of the kernel function for particle  $i$  and satisfies  $\nabla_i W_{ij} = -\nabla_j W_{ij}$ , and  $m_j$  and  $\rho_j$  are the mass and density of particle  $j$ , respectively. If we denote

$m_j / \rho_j = V_j$  to represent the volume associated with particle  $j$ , the particle number density  $n_j$  can be defined as  $n_j = 1 / V_j$ , i.e., the number of particles per unit volume. Following Tartakovsky and Meakin (2005), we have  $n_j = \sum_k W(\mathbf{x}_j - \mathbf{x}_k, h)$ , where  $\mathbf{x}_k$  is the location of neighbor particles of particle  $j$ .

Eq. (8) has a potential problem that, for a constant  $C$  in space,  $\langle \nabla C_i \rangle$  should be zero theoretically but  $\sum_{j=1}^{N_b} (m_j / \rho_j) \nabla_i W_{ij} = 0$  may not be numerically satisfied. To resolve this problem, Monaghan (2005) expressed  $\nabla C_i$  as

$$\nabla C_i = \frac{1}{\Phi_i} (\nabla(\Phi_i C_i) - C_i \nabla \Phi_i) \quad (9)$$

where  $\Phi_i = \Phi(\mathbf{x}_i)$  can be any differentiable function. With Eq. (9),  $\nabla C_i$  can be approximated as (Monaghan, 2005)

$$\langle \nabla C_i \rangle = \frac{1}{\Phi_i} \sum_j^{N_b} \frac{m_j}{\rho_j} \Phi_j (C_j - C_i) \nabla_i W_{ij} \quad (10)$$

Choosing  $\Phi_i = 1$  leads to

$$\langle \nabla C_i \rangle = \sum_j^{N_b} \frac{m_j}{\rho_j} (C_j - C_i) \nabla_i W_{ij} \quad (11)$$

Eq. (11) is commonly used in SPH, since it improves particle approximation accuracy (Liu and Liu, 2006). For this reason, this study used Eq. (11) rather than Eq. (8).

Numerical accuracy of SPH depends on the two particle approximations defined in Eqs. (7) and (11) for  $C$  and  $\nabla C$ , respectively. Accuracy of Eq. (7) is closely related to the unity and symmetric properties of the kernel function, and accuracy of Eq. (11) depends on the anti-symmetric property of the kernel's first-order derivatives. To show these, we apply the Taylor series expansion to  $C_j = C(\mathbf{x}_j)$  at particle location  $\mathbf{x}_i = \{\mathbf{x}_b, \mathbf{y}_b, \mathbf{z}_b\}$ , and retain the first-order derivatives, i.e.,

$$C_j \approx C_i + (\mathbf{x}_j^\alpha - \mathbf{x}_i^\alpha) \frac{\partial C_i}{\partial \mathbf{x}_i^\alpha} = C_i + (x_j - x_i) \frac{\partial C_i}{\partial x_i} + (y_j - y_i) \frac{\partial C_i}{\partial y_i} + (z_j - z_i) \frac{\partial C_i}{\partial z_i} \quad (12)$$

where  $\alpha$  is a dimension index for the  $x$ ,  $y$ , and  $z$  directions. To analyze the error of the particle approximation given in Eq. (7), we substitute Eq. (12) to Eq. (7), and have

$$\langle C_i \rangle = \sum_{j=1}^{N_b} \frac{m_j}{\rho_j} C_j W_{ij} \approx C_i \sum_{j=1}^{N_b} \frac{m_j}{\rho_j} W_{ij} + \frac{\partial C(\mathbf{x}_i^\alpha)}{\partial \mathbf{x}_i^\alpha} \sum_{j=1}^{N_b} \frac{m_j}{\rho_j} (\mathbf{x}_j^\alpha - \mathbf{x}_i^\alpha) W_{ij} \quad (13)$$

If the unity property  $\sum_{j=1}^{N_b} \frac{m_j}{\rho_j} W_{ij} = 1$  and the symmetric property  $\sum_{j=1}^{N_b} \frac{m_j}{\rho_j} (\mathbf{x}_j^\alpha - \mathbf{x}_i^\alpha) W_{ij} = 0$  are satisfied, then Eq. (13) becomes  $\langle C_i \rangle \approx C_i$  with a second-order accuracy in terms of  $r = |\mathbf{x}_j - \mathbf{x}_i|$ , where  $r$  is the distance between particles  $i$  and  $j$ .

Whether the unity and symmetric properties of a kernel function are satisfied depends on spatial distribution of the particles. This is illustrated in Fig. 1 with uniform and irregular particle distributions for a one-dimensional problem. For the uniform distribution, any two neighbor particles have the same distance of  $\Delta x = 0.125$  m. Based on the kernel function defined in Eq. (6), set  $h = 2\Delta x$ , the radius of the support domain  $\Omega$  as  $2h = 4\Delta x$ , and  $W_0 = 1/h$  for the one-dimensional problem. Fig. 1(a1) show functions  $W_{ij}/W_0$  and  $(x_j - x_i)W_{ij}$  as a function of  $(x_j - x_i)/h$  for a number of uniformly distributed particles; Fig. 1(a2) is similar to Fig. 1(a1) but for irregularly distributed particles. The irregular particle distribution is generated by adding random noises to the uniformly

distributed particles; the random noises follow a uniform distribution within the range of  $[0, \Delta x]$ . In the two figures, the dashed lines represent analytical values of  $W_{ij}/W_0$  and  $(x_j - x_i)W_{ij}$  based on Eq. (6). The area in blue corresponds to  $\sum_{j=1}^{N_b} \frac{m_j}{\rho_j} W_{ij}$ , and the area in fuchsia corresponds to  $\sum_{j=1}^{N_b} \frac{m_j}{\rho_j} (\mathbf{x}_j^\alpha - \mathbf{x}_i^\alpha) W_{ij}$ . In Fig. 1(a1) for the uniformly distributed particles, with  $h = 2\Delta x$  and  $N_b = 7$  for the support domain of  $(-2h, 2h)$ , the blue area estimated via  $\sum_{j=1}^{N_b} \frac{m_j}{\rho_j} W_{ij} = \sum_{j=1}^{N_b} \frac{1}{\rho_j} W_{ij}$  equals 1.0000, indicating that the unit property is satisfied. The number,  $n_j$ , of particles per unit volume is evaluated as  $n_j = \sum_k W(\mathbf{x}_j - \mathbf{x}_k, h)$  by following Tartakovsky and Meakin (2005). This is the case for the entire manuscript. The fuchsia area estimated via  $\sum_{j=1}^{N_b} \frac{m_j}{\rho_j} (\mathbf{x}_j^\alpha - \mathbf{x}_i^\alpha) W_{ij} = \sum_{j=1}^{N_b} \frac{1}{\rho_j} (\mathbf{x}_j^\alpha - \mathbf{x}_i^\alpha) W_{ij}$  equals 0.0000, indicating that the symmetric property is satisfied. In Fig. 1(a2) for the irregularly distributed particles, with  $h = 2\Delta x$  and  $N_b = 8$  for the support domain of  $(-2h, 2h)$ , similar to the estimation for the uniformly distributed particles, we have  $\sum_{j=1}^{N_b} \frac{m_j}{\rho_j} W_{ij} = 1.0457$  and  $\sum_{j=1}^{N_b} \frac{m_j}{\rho_j} (\mathbf{x}_j^\alpha - \mathbf{x}_i^\alpha) W_{ij} = 0.0067$ , indicating that the unity and symmetric properties of the kernel are not satisfied. This is not surprising, if one examines the distributions of the particles and the shapes of  $W_{ij}/W_0$  and  $(x_j - x_i)W_{ij}$  based on the particle distributions. Because the particles are irregularly distributed, the shapes of the  $W_{ij}/W_0$  and  $(x_j - x_i)W_{ij}$  functions cannot be accurately approximated. This is the reason that, for irregularly distributed particles, the SPH-based approximation of a function may not be accurate.

To have an accurate particle approximation of the first-order derivatives of concentration, the first-order derivatives of the kernel need to satisfy the so-called anti-symmetric property (Chen and Beraun, 2000). Taking the first-order derivatives of  $C_i$  in the  $x$  direction as an example, based on Eq. (11) of the derivative and Eq. (12) of the Taylor series expansion of  $C_j$ , we have

$$\begin{aligned} \left\langle \frac{\partial C_i}{\partial x_i} \right\rangle &= \sum_{j=1}^{N_b} \frac{m_j}{\rho_j} (C_j - C_i) \frac{\partial W_{ij}}{\partial x_i} \\ &\approx \frac{\partial C_i}{\partial x_i} \sum_{j=1}^{N_b} \frac{m_j}{\rho_j} x_{ji} \frac{\partial W_{ij}}{\partial x_i} + \frac{\partial C_i}{\partial y_i} \sum_{j=1}^{N_b} \frac{m_j}{\rho_j} y_{ji} \frac{\partial W_{ij}}{\partial x_i} + \frac{\partial C_i}{\partial z_i} \sum_{j=1}^{N_b} \frac{m_j}{\rho_j} z_{ji} \frac{\partial W_{ij}}{\partial x_i} \end{aligned} \quad (14)$$

where  $x_{ji} = x_j - x_i$ ,  $y_{ji} = y_j - y_i$ , and  $z_{ji} = z_j - z_i$ . The anti-symmetric property for the first-order derivative of the kernel in the  $x$  direction is as follows:  $\sum_{j=1}^{N_b} \frac{m_j}{\rho_j} x_{ji} \frac{\partial W_{ij}}{\partial x_i} = 1$ ,  $\sum_{j=1}^{N_b} \frac{m_j}{\rho_j} y_{ji} \frac{\partial W_{ij}}{\partial x_i} = 0$  and  $\sum_{j=1}^{N_b} \frac{m_j}{\rho_j} z_{ji} \frac{\partial W_{ij}}{\partial x_i} = 0$ . If the three equations are satisfied, then  $\langle \frac{\partial C_i}{\partial x_i} \rangle \approx \frac{\partial C(x_i)}{\partial x_i}$  with a second-order accuracy in terms of  $r = |\mathbf{x}_j - \mathbf{x}_i|$ , where  $r$  is the distance between particles  $i$  and  $j$  (Liu and Liu, 2010).

The anti-symmetric property may not be satisfied for irregularly distributed particle, and this is demonstrated in Figs. 1(a3) and 1(a4) for function  $(x_j - x_i)W_{i,x}/W_0$ , which is  $x_{ji} \frac{\partial W_{ij}}{\partial x_i}$  normalized by  $W_0$  because the  $x$ -axis is multiplied by  $W_0 = 1/h$ . The two figures are plotted using the same kernel function and particle distribution used for plotting Figs. 1(a1) and 1(a2). For this one-dimensional problem, we only examine whether  $\sum_{j=1}^{N_b} \frac{m_j}{\rho_j} x_{ji} \frac{\partial W_{ij}}{\partial x_i} = 1$  is satisfied, i.e., whether the areas in red in Figs. 1(a3) and 1(a4) equal 1. For Fig. 1(a3) with the uniformly distributed particles,  $\sum_{j=1}^{N_b} \frac{m_j}{\rho_j} x_{ji} \frac{\partial W_{ij}}{\partial x_i} = 0.9999$ , which is close to 1. For Fig. 1(a4) with the irregularly distributed particles, this term becomes 0.8060, indicating that the anti-symmetric property is not satisfied. The two figures demonstrate that, for irregularly distributed particles, the SPH-based approximations of the first-order derivatives of concentration may not be accurate.

## 2.2. Solving ADE by using SPH

The numerical errors of SPH caused by irregularly distributed particles affects accuracy of the SPH-solutions of the ADE. Based on the SPH solution of the heat-conduction equation (Cleary and Monaghan, 1999), Espanol and Revenga (2003) derived the SPH integral approximation of dispersive fluxes. According to Alvarado-Rodríguez et al. (2019) and Herrera et al. (2009), the SPH approximation of Eq. (3) for particle  $i$  is given as

$$\frac{dC_i}{dt} = \frac{1}{2} \sum_{j=1}^{N_b} \frac{1}{n_{ij}} (C_j - C_i) \frac{\mathbf{x}_j - \mathbf{x}_i}{|\mathbf{x}_j - \mathbf{x}_i|^2} \nabla_i W_{ij} \left[ \sum_{\alpha} \sum_{\beta} \left( D_{\alpha\beta}^i + D_{\alpha\beta}^j \right) \left( \Gamma \frac{(\mathbf{x}_j - \mathbf{x}_i)_\alpha (\mathbf{x}_j - \mathbf{x}_i)_\beta}{|\mathbf{x}_j - \mathbf{x}_i|^2} - \delta_{\alpha\beta} \right) \right] \quad (15)$$

where  $n_{ij} = 2n_i n_j / (n_i + n_j)$  is the harmonic mean of  $n_i$  and  $n_j$  that are the particle density number at positions  $\mathbf{x}_i$  and  $\mathbf{x}_j$ , respectively,  $\Gamma = 4$  and 5 in a two- and three-dimensional space, respectively (Espanol and Revenga, 2003; Yildiz et al., 2009),  $\alpha$  and  $\beta$  are the dimension indices ranging from 1 to 3 (i.e., from  $x$  to  $z$ ),  $D_{\alpha\beta}^i$  is a component of the dispersion coefficient tensor related to particle  $i$ , and  $\delta_{\alpha\beta}$  is the Kronecker delta function. To obtain the solution of  $C$  in time, this study solves Eq. (15) numerically using the algorithm of predictor-corrector leapfrog

$$\left\{ \begin{array}{l} \sum_{j=1}^{N_b} \frac{m_j}{\rho_j} C_j \frac{\partial W_{ij}}{\partial x_i} = \sum_{j=1}^{N_b} \frac{m_j}{\rho_j} C_i \frac{\partial W_{ij}}{\partial x_i} + \frac{\partial C_i}{\partial x_i} \sum_{j=1}^{N_b} \frac{m_j}{\rho_j} x_{ji} \frac{\partial W_{ij}}{\partial x_i} + \frac{\partial C_i}{\partial y_i} \sum_{j=1}^{N_b} \frac{m_j}{\rho_j} y_{ji} \frac{\partial W_{ij}}{\partial x_i} + \frac{\partial C_i}{\partial z_i} \sum_{j=1}^{N_b} \frac{m_j}{\rho_j} z_{ji} \frac{\partial W_{ij}}{\partial x_i} \\ \sum_{j=1}^{N_b} \frac{m_j}{\rho_j} C_j \frac{\partial W_{ij}}{\partial y_i} = \sum_{j=1}^{N_b} \frac{m_j}{\rho_j} C_i \frac{\partial W_{ij}}{\partial y_i} + \frac{\partial C_i}{\partial x_i} \sum_{j=1}^{N_b} \frac{m_j}{\rho_j} x_{ji} \frac{\partial W_{ij}}{\partial y_i} + \frac{\partial C_i}{\partial y_i} \sum_{j=1}^{N_b} \frac{m_j}{\rho_j} y_{ji} \frac{\partial W_{ij}}{\partial y_i} + \frac{\partial C_i}{\partial z_i} \sum_{j=1}^{N_b} \frac{m_j}{\rho_j} z_{ji} \frac{\partial W_{ij}}{\partial y_i} \\ \sum_{j=1}^{N_b} \frac{m_j}{\rho_j} C_j \frac{\partial W_{ij}}{\partial z_i} = \sum_{j=1}^{N_b} \frac{m_j}{\rho_j} C_i \frac{\partial W_{ij}}{\partial z_i} + \frac{\partial C_i}{\partial x_i} \sum_{j=1}^{N_b} \frac{m_j}{\rho_j} x_{ji} \frac{\partial W_{ij}}{\partial z_i} + \frac{\partial C_i}{\partial y_i} \sum_{j=1}^{N_b} \frac{m_j}{\rho_j} y_{ji} \frac{\partial W_{ij}}{\partial z_i} + \frac{\partial C_i}{\partial z_i} \sum_{j=1}^{N_b} \frac{m_j}{\rho_j} z_{ji} \frac{\partial W_{ij}}{\partial z_i} \end{array} \right. \quad (16)$$

time integration, which is computationally efficient and does not require a large amount of computer memory (Alvarado-Rodríguez et al., 2019). In the predictor step, the particle position and associated solute con-

velocity  $v$ ) and the derivative of concentration at the half time step. Afterward, in the prediction step, the particle position and solute concentration are advanced for the full time step using the derivatives calculated at the half time step. Since the derivation of Eq. (15) involves the particle approximations of  $C_i$  and its first-order derivatives, accuracy of Eq. (15) depends on particle distributions, as discussed above. For an irregular particle distribution, SPH accuracy improvement is needed by using the FPM method.

## 2.3. Finite particle method (FPM) and FPM solution of ADE

In comparison with SPH, FPM is less sensitive to spatial distribution of particles. This is achieved by correcting the first-order derivatives of the kernel function involved in Eq. (15). Following Xu and Deng (2016), we first multiply the both sides of Eq. (12) by the three first-order derivatives,  $\partial W_{ij}/\partial x_i$ ,  $\partial W_{ij}/\partial y_i$ , and  $\partial W_{ij}/\partial z_i$ , and then integrate over the support domain. Subsequently replacing the integrations with the particle approximations leads to

Moving the first term on the right-hand side of Eq. (16) to the left-hand side gives

$$\left\{ \begin{array}{l} \left\langle \frac{\partial C_i}{\partial x_i} \right\rangle = \sum_{j=1}^{N_b} \frac{m_j}{\rho_j} (C_j - C_i) \frac{\partial W_{ij}}{\partial x_i} = \frac{\partial C_i}{\partial x_i} \sum_{j=1}^{N_b} \frac{m_j}{\rho_j} x_{ji} \frac{\partial W_{ij}}{\partial x_i} + \frac{\partial C_i}{\partial y_i} \sum_{j=1}^{N_b} \frac{m_j}{\rho_j} y_{ji} \frac{\partial W_{ij}}{\partial x_i} + \frac{\partial C_i}{\partial z_i} \sum_{j=1}^{N_b} \frac{m_j}{\rho_j} z_{ji} \frac{\partial W_{ij}}{\partial x_i} \\ \left\langle \frac{\partial C_i}{\partial y_i} \right\rangle = \sum_{j=1}^{N_b} \frac{m_j}{\rho_j} (C_j - C_i) \frac{\partial W_{ij}}{\partial y_i} = \frac{\partial C_i}{\partial x_i} \sum_{j=1}^{N_b} \frac{m_j}{\rho_j} x_{ji} \frac{\partial W_{ij}}{\partial y_i} + \frac{\partial C_i}{\partial y_i} \sum_{j=1}^{N_b} \frac{m_j}{\rho_j} y_{ji} \frac{\partial W_{ij}}{\partial y_i} + \frac{\partial C_i}{\partial z_i} \sum_{j=1}^{N_b} \frac{m_j}{\rho_j} z_{ji} \frac{\partial W_{ij}}{\partial y_i} \\ \left\langle \frac{\partial C_i}{\partial z_i} \right\rangle = \sum_{j=1}^{N_b} \frac{m_j}{\rho_j} (C_j - C_i) \frac{\partial W_{ij}}{\partial z_i} = \frac{\partial C_i}{\partial x_i} \sum_{j=1}^{N_b} \frac{m_j}{\rho_j} x_{ji} \frac{\partial W_{ij}}{\partial z_i} + \frac{\partial C_i}{\partial y_i} \sum_{j=1}^{N_b} \frac{m_j}{\rho_j} y_{ji} \frac{\partial W_{ij}}{\partial z_i} + \frac{\partial C_i}{\partial z_i} \sum_{j=1}^{N_b} \frac{m_j}{\rho_j} z_{ji} \frac{\partial W_{ij}}{\partial z_i} \end{array} \right. \quad (17)$$

centration of the particle are advanced in a half time step, and the results are used to evaluate time derivative of particle position (i.e., seepage

Writing Eq. (17) in the matrix form, we have the particle approximations

as

$$\begin{bmatrix} \left\langle \frac{\partial C_i}{\partial x_i} \right\rangle \\ \left\langle \frac{\partial C_i}{\partial y_i} \right\rangle \\ \left\langle \frac{\partial C_i}{\partial z_i} \right\rangle \end{bmatrix} = \begin{bmatrix} \sum_{j=1}^{N_b} \frac{m_j}{\rho_j} (C_j - C_i) \frac{\partial W_{ij}}{\partial x_i} \\ \sum_{j=1}^{N_b} \frac{m_j}{\rho_j} (C_j - C_i) \frac{\partial W_{ij}}{\partial y_i} \\ \sum_{j=1}^{N_b} \frac{m_j}{\rho_j} (C_j - C_i) \frac{\partial W_{ij}}{\partial z_i} \end{bmatrix} = \begin{bmatrix} \sum_{j=1}^{N_b} \frac{m_j}{\rho_j} x_{ji} \frac{\partial W_{ij}}{\partial x_i} & \sum_{j=1}^{N_b} \frac{m_j}{\rho_j} y_{ji} \frac{\partial W_{ij}}{\partial x_i} & \sum_{j=1}^{N_b} \frac{m_j}{\rho_j} z_{ji} \frac{\partial W_{ij}}{\partial x_i} \\ \sum_{j=1}^{N_b} \frac{m_j}{\rho_j} x_{ji} \frac{\partial W_{ij}}{\partial y_i} & \sum_{j=1}^{N_b} \frac{m_j}{\rho_j} y_{ji} \frac{\partial W_{ij}}{\partial y_i} & \sum_{j=1}^{N_b} \frac{m_j}{\rho_j} z_{ji} \frac{\partial W_{ij}}{\partial y_i} \\ \sum_{j=1}^{N_b} \frac{m_j}{\rho_j} x_{ji} \frac{\partial W_{ij}}{\partial z_i} & \sum_{j=1}^{N_b} \frac{m_j}{\rho_j} y_{ji} \frac{\partial W_{ij}}{\partial z_i} & \sum_{j=1}^{N_b} \frac{m_j}{\rho_j} z_{ji} \frac{\partial W_{ij}}{\partial z_i} \end{bmatrix} \begin{bmatrix} \frac{\partial C_i}{\partial x_i} \\ \frac{\partial C_i}{\partial y_i} \\ \frac{\partial C_i}{\partial z_i} \end{bmatrix} \quad (18)$$

This leads to the expression of the three first-order derivatives of  $C_i$  as

$$\begin{bmatrix} \frac{\partial C_i}{\partial x_i} \\ \frac{\partial C_i}{\partial y_i} \\ \frac{\partial C_i}{\partial z_i} \end{bmatrix} = \mathbf{M}^{-1} \begin{bmatrix} \sum_{j=1}^{N_b} \frac{m_j}{\rho_j} (C_j - C_i) \frac{\partial W_{ij}}{\partial x_i} \\ \sum_{j=1}^{N_b} \frac{m_j}{\rho_j} (C_j - C_i) \frac{\partial W_{ij}}{\partial y_i} \\ \sum_{j=1}^{N_b} \frac{m_j}{\rho_j} (C_j - C_i) \frac{\partial W_{ij}}{\partial z_i} \end{bmatrix} = \begin{bmatrix} \sum_{j=1}^{N_b} \frac{m_j}{\rho_j} x_{ji} \frac{\partial W_{ij}}{\partial x_i} & \sum_{j=1}^{N_b} \frac{m_j}{\rho_j} y_{ji} \frac{\partial W_{ij}}{\partial x_i} & \sum_{j=1}^{N_b} \frac{m_j}{\rho_j} z_{ji} \frac{\partial W_{ij}}{\partial x_i} \\ \sum_{j=1}^{N_b} \frac{m_j}{\rho_j} x_{ji} \frac{\partial W_{ij}}{\partial y_i} & \sum_{j=1}^{N_b} \frac{m_j}{\rho_j} y_{ji} \frac{\partial W_{ij}}{\partial y_i} & \sum_{j=1}^{N_b} \frac{m_j}{\rho_j} z_{ji} \frac{\partial W_{ij}}{\partial y_i} \\ \sum_{j=1}^{N_b} \frac{m_j}{\rho_j} x_{ji} \frac{\partial W_{ij}}{\partial z_i} & \sum_{j=1}^{N_b} \frac{m_j}{\rho_j} y_{ji} \frac{\partial W_{ij}}{\partial z_i} & \sum_{j=1}^{N_b} \frac{m_j}{\rho_j} z_{ji} \frac{\partial W_{ij}}{\partial z_i} \end{bmatrix}^{-1} \begin{bmatrix} \sum_{j=1}^{N_b} \frac{m_j}{\rho_j} (C_j - C_i) \frac{\partial W_{ij}}{\partial x_i} \\ \sum_{j=1}^{N_b} \frac{m_j}{\rho_j} (C_j - C_i) \frac{\partial W_{ij}}{\partial y_i} \\ \sum_{j=1}^{N_b} \frac{m_j}{\rho_j} (C_j - C_i) \frac{\partial W_{ij}}{\partial z_i} \end{bmatrix} \quad (19)$$

where

$$\mathbf{M} = \begin{bmatrix} \sum_j \frac{m_j}{\rho_j} x_{ji} \frac{\partial W_{ij}}{\partial x_i} & \sum_j \frac{m_j}{\rho_j} y_{ji} \frac{\partial W_{ij}}{\partial x_i} & \sum_j \frac{m_j}{\rho_j} z_{ji} \frac{\partial W_{ij}}{\partial x_i} \\ \sum_j \frac{m_j}{\rho_j} x_{ji} \frac{\partial W_{ij}}{\partial y_i} & \sum_j \frac{m_j}{\rho_j} y_{ji} \frac{\partial W_{ij}}{\partial y_i} & \sum_j \frac{m_j}{\rho_j} z_{ji} \frac{\partial W_{ij}}{\partial y_i} \\ \sum_j \frac{m_j}{\rho_j} x_{ji} \frac{\partial W_{ij}}{\partial z_i} & \sum_j \frac{m_j}{\rho_j} y_{ji} \frac{\partial W_{ij}}{\partial z_i} & \sum_j \frac{m_j}{\rho_j} z_{ji} \frac{\partial W_{ij}}{\partial z_i} \end{bmatrix} \quad (20)$$

If the anti-symmetric property of the kernel function discussed in Section 2.1 is satisfied, matrix  $\mathbf{M}$  is the identity matrix, and the particle approximations of the first-order derivatives of  $C_i$  in Eq. (19) have the second-order accuracy in terms of  $r = |\mathbf{x}_j - \mathbf{x}_i|$ . The anti-symmetric property however may not hold for irregularly distributed particles, as discussed in Section 2.1.

To resolve the problem related to the anti-symmetric property, FPM assumes that there exists a modified kernel gradient,  $\frac{\partial^M W_{ij}}{\partial \mathbf{x}_i}$ . Using the modified kernel gradient and based on Eq. (11), we can write the particle approximation of the first-order derivatives of  $C_i$  as

$$\left\langle \frac{\partial C_i}{\partial \mathbf{x}_i} \right\rangle = \sum_{j=1}^{N_b} \frac{m_j}{\rho_j} (C_j - C_i) \frac{\partial^M W_{ij}}{\partial \mathbf{x}_i} \quad (21)$$

Based on Eqs. (19) and (21), setting  $\left\langle \frac{\partial C_i}{\partial \mathbf{x}_i} \right\rangle = \frac{\partial C_i}{\partial \mathbf{x}_i}$  gives

$$\begin{bmatrix} \sum_{j=1}^{N_b} \frac{m_j}{\rho_j} (C_j - C_i) \frac{\partial^M W_{ij}}{\partial x_i} \\ \sum_{j=1}^{N_b} \frac{m_j}{\rho_j} (C_j - C_i) \frac{\partial^M W_{ij}}{\partial y_i} \\ \sum_{j=1}^{N_b} \frac{m_j}{\rho_j} (C_j - C_i) \frac{\partial^M W_{ij}}{\partial z_i} \end{bmatrix} =$$

$$\begin{bmatrix} \sum_{j=1}^{N_b} \frac{m_j}{\rho_j} x_{ji} \frac{\partial W_{ij}}{\partial x_i} & \sum_{j=1}^{N_b} \frac{m_j}{\rho_j} y_{ji} \frac{\partial W_{ij}}{\partial x_i} & \sum_{j=1}^{N_b} \frac{m_j}{\rho_j} z_{ji} \frac{\partial W_{ij}}{\partial x_i} \\ \sum_{j=1}^{N_b} \frac{m_j}{\rho_j} x_{ji} \frac{\partial W_{ij}}{\partial y_i} & \sum_{j=1}^{N_b} \frac{m_j}{\rho_j} y_{ji} \frac{\partial W_{ij}}{\partial y_i} & \sum_{j=1}^{N_b} \frac{m_j}{\rho_j} z_{ji} \frac{\partial W_{ij}}{\partial y_i} \\ \sum_{j=1}^{N_b} \frac{m_j}{\rho_j} x_{ji} \frac{\partial W_{ij}}{\partial z_i} & \sum_{j=1}^{N_b} \frac{m_j}{\rho_j} y_{ji} \frac{\partial W_{ij}}{\partial z_i} & \sum_{j=1}^{N_b} \frac{m_j}{\rho_j} z_{ji} \frac{\partial W_{ij}}{\partial z_i} \end{bmatrix}^{-1} \begin{bmatrix} \sum_{j=1}^{N_b} \frac{m_j}{\rho_j} (C_j - C_i) \frac{\partial W_{ij}}{\partial x_i} \\ \sum_{j=1}^{N_b} \frac{m_j}{\rho_j} (C_j - C_i) \frac{\partial W_{ij}}{\partial y_i} \\ \sum_{j=1}^{N_b} \frac{m_j}{\rho_j} (C_j - C_i) \frac{\partial W_{ij}}{\partial z_i} \end{bmatrix} \quad (22)$$

This leads to the modified kernel gradients as

$$\begin{bmatrix} \frac{\partial^M W_{ij}}{\partial x_i} \\ \frac{\partial^M W_{ij}}{\partial y_i} \\ \frac{\partial^M W_{ij}}{\partial z_i} \end{bmatrix} = \begin{bmatrix} \sum_{j=1}^{N_b} \frac{m_j}{\rho_j} x_{ji} \frac{\partial W_{ij}}{\partial x_i} & \sum_{j=1}^{N_b} \frac{m_j}{\rho_j} y_{ji} \frac{\partial W_{ij}}{\partial x_i} & \sum_{j=1}^{N_b} \frac{m_j}{\rho_j} z_{ji} \frac{\partial W_{ij}}{\partial x_i} \\ \sum_{j=1}^{N_b} \frac{m_j}{\rho_j} x_{ji} \frac{\partial W_{ij}}{\partial y_i} & \sum_{j=1}^{N_b} \frac{m_j}{\rho_j} y_{ji} \frac{\partial W_{ij}}{\partial y_i} & \sum_{j=1}^{N_b} \frac{m_j}{\rho_j} z_{ji} \frac{\partial W_{ij}}{\partial y_i} \\ \sum_{j=1}^{N_b} \frac{m_j}{\rho_j} x_{ji} \frac{\partial W_{ij}}{\partial z_i} & \sum_{j=1}^{N_b} \frac{m_j}{\rho_j} y_{ji} \frac{\partial W_{ij}}{\partial z_i} & \sum_{j=1}^{N_b} \frac{m_j}{\rho_j} z_{ji} \frac{\partial W_{ij}}{\partial z_i} \end{bmatrix}^{-1} \begin{bmatrix} \frac{\partial W_{ij}}{\partial x_i} \\ \frac{\partial W_{ij}}{\partial y_i} \\ \frac{\partial W_{ij}}{\partial z_i} \end{bmatrix} = \mathbf{M}^{-1} \begin{bmatrix} \frac{\partial W_{ij}}{\partial x_i} \\ \frac{\partial W_{ij}}{\partial y_i} \\ \frac{\partial W_{ij}}{\partial z_i} \end{bmatrix} \quad (23)$$

Expressing Eq. (23) in a matrix form gives the modified kernel gradient as

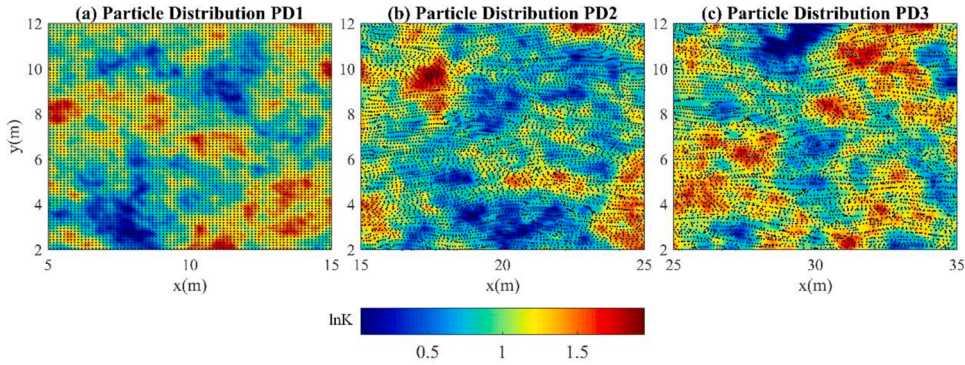


**Fig. 2.** Illustration of three particle distributions, PD1-PD3, used for the first numerical case with  $\sigma_{\ln K}^2 = 0.1$ . In the background, the log hydraulic conductivity field. The integral scale,  $I_{\ln K}$ , of heterogeneous hydraulic conductivity field is set as  $I_{\ln K} = 8\Delta x = 1$  m.

$$\nabla_i^M W_{ij} = \mathbf{M}^{-1} \nabla_i W_{ij} \quad (24)$$

With this modified kernel gradient, in FPM, the gradient of concentration is approximated by using Eq. (21) rather than Eq. (11). Accordingly, Eq. (15) becomes

$$\frac{dC_i}{dt} = \frac{1}{2} \sum_{j=1}^{N_b} \frac{1}{n_{ij}} (C_j - C_i) \frac{\mathbf{x}_j - \mathbf{x}_i}{|\mathbf{x}_j - \mathbf{x}_i|^2} \nabla_i^M W_{ij} \left[ \sum_{\alpha} \sum_{\beta} \left( D_{\alpha\beta}^i + D_{\beta\alpha}^i \right) \left( \Gamma \frac{(\mathbf{x}_j - \mathbf{x}_i)_\alpha (\mathbf{x}_j - \mathbf{x}_i)_\beta}{|\mathbf{x}_j - \mathbf{x}_i|^2} - \delta_{\alpha\beta} \right) \right] \quad (25)$$

and it provides the FPM solution of the ADE. The only difference between Eqs. (15) and (25) is the use of the modified kernel gradient corrected by using matrix  $\mathbf{M}$ . This is an advantage of FPM, because Eq. (25) of FPM can be implemented in a straightforward way based on Eq. (15) of the SPH implementation. When  $\mathbf{M}$  is a unity matrix, the FPM implementation is identical to the SPH implementation.

Fig. 1(b) illustrates why FPM can yield more accurate results than SPH for irregularly distributed particles. Fig. 1(b) uses the same particles used for plotting Fig. 1(a4) but uses the modified first-order derivative of the kernel function, i.e.,  $(\mathbf{x}_j - \mathbf{x}_i)W_{i,x}^M / W_0$ . Without the modified derivative,  $\sum_{j=1}^{N_b} \frac{m_j}{\rho_j} x_{ji} \frac{\partial W_{ij}}{\partial x_i} = 0.8060$  (Fig. 1(a4)); with the modified kernel derivative,  $\sum_{j=1}^{N_b} \frac{m_j}{\rho_j} x_{ji} \frac{\partial^M W_{ij}}{\partial x_i} = 1.0000$ . Fig. 1(b) shows that the modified kernel derivative produces an extra area in the right half of the function to compensate the missing area in the left half of the function. The extent of this compensation depends on the level of irregularity of particle distributions. For extremely irregular particles, FPM results may still be inaccurate, as shown in the numerical examples discussed in Section 3.

The modified kernel gradient,  $\nabla_i^M W_{ij}$ , can be obtained by using Eq. (24) or solving a system of equation,  $\mathbf{M} \nabla_i^M W_{ij} = \nabla_i W_{ij}$ ; the latter approach is used in this study. Either approach makes FPM more computationally expensive than SPH. More importantly, if the matrix is ill-conditioned or even singular for cases with highly irregular particles, FPM may suffer from numerical instability or early termination (Liu and Liu, 2010). This occurs in the numerical experiments in Section 3 of this study when FPM is used to simulate a solute transport problem with both

diffusion and advection dispersion in a heterogeneous field of hydraulic conductivity. To resolve this problem, we adopt the decoupled FPM method developed by Zhang and Liu (2018). The method uses matrix  $\bar{\mathbf{M}}$ ,

$$\bar{\mathbf{M}} = \begin{bmatrix} \sum_j \frac{m_j}{\rho_j} x_{ji} \frac{\partial W_{ij}}{\partial x_i} & 0 & 0 \\ 0 & \sum_j \frac{m_j}{\rho_j} y_{ji} \frac{\partial W_{ij}}{\partial y_i} & 0 \\ 0 & 0 & \sum_j \frac{m_j}{\rho_j} z_{ji} \frac{\partial W_{ij}}{\partial z_i} \end{bmatrix} \quad (26)$$

which contains only the diagonal elements of  $\mathbf{M}$ . Using  $\bar{\mathbf{M}}$  assumes that the diagonal elements of  $\mathbf{M}$  dominate over the off-diagonal terms, e.g.,  $\sum_j^{N_b} \frac{m_j}{\rho_j} x_{ji} \frac{\partial W_{ij}}{\partial x_i}$  dominates over the other two terms,  $\sum_j^{N_b} \frac{m_j}{\rho_j} y_{ji} \frac{\partial W_{ij}}{\partial x_i}$  and  $\sum_j^{N_b} \frac{m_j}{\rho_j} z_{ji} \frac{\partial W_{ij}}{\partial x_i}$ , in the first row of matrix  $\mathbf{M}$ . Evaluating the inverse of the diagonal matrix,  $\bar{\mathbf{M}}$ , or solving  $\bar{\mathbf{M}} \nabla_i^M W_{ij} = \nabla_i W_{ij}$  is straightforward and computationally efficient. In this study, if  $\mathbf{M} \nabla_i^M W_{ij} = \nabla_i W_{ij}$  cannot be solved for a particle due to ill-conditioned  $\mathbf{M}$  associated with the particle, the decoupled FPM is used for the particle by solving  $\bar{\mathbf{M}} \nabla_i^M W_{ij} = \nabla_i W_{ij}$ .

#### 2.4. Particle approximation errors with irregular particle distributions

In this section, we briefly describe the approximation errors of SPH with irregular particle distributions. According to Monaghan (2005), meshfree approximations in SPH based on the kernel interpolant integration has two sources of errors: the smoothing error caused by the integral interpolation and the discretizing error caused by the

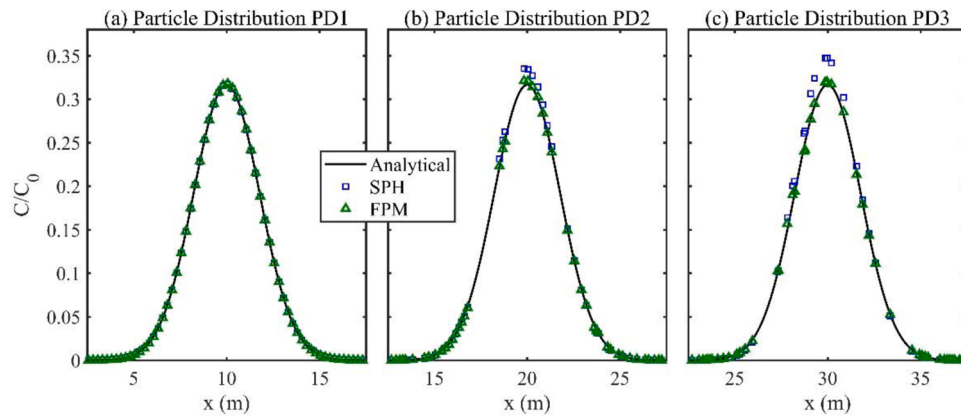


**Fig. 3.** Profiles of the analytical, SPH, and FPM solutions of normalized concentration ( $C/C_0$ ) along the line of  $y = 7$  m for particle distributions PD1 – PD3 with  $\sigma_{\text{r}_i K}^2 = 0.1$ . Normalized concentration in this figure is based on the discrete particles.

summation of discrete particle in the integral. The smoothing error depends on the shape and smoothing length of the kernel function; using a small  $h$  value can reduce the smoothing error (Monaghan, 2005; Zhu et al., 2015). The discretizing error depends on the particle number and particle distribution. For uniformly distributed particle, generally speaking, using small  $h$  leads to small discretizing error. For irregularly distributed particle, using a small  $h$  value may result in a small number of neighbor particles in the corresponding support domain, and thus increases discretizing error (Zhu et al., 2015; Sigalotti et al., 2016; Herrera and Beckie, 2013). To simultaneously reduce smoothing and discretizing errors requires decreasing the smoothing length and simultaneously increasing the number of particles, so that the number of particles per support domain does not change on an average sense for all particles (Zhu et al., 2015). This however is difficult to achieve in practice for an irregular particle distribution, because it is difficult to estimate the number of particles within a support domain for irregularly distributed particles (Herrera et al., 2009). For the same reason, it is also difficult to use a variable smoothing length as a potential alternative solution to ensure a stable average number of neighbor particles. The tradeoff between the smoothing error and the discretizing error must be considered when determining  $h$  values.

When using SPH or FPM to solve ADE with heterogeneous hydraulic conductivity, the particle approximation errors increase with time, because the degree of particle irregularity increases with time. Generally speaking, the initial particle distribution is always uniform. Therefore, at an early time, the particle distribution is still uniform, and the smoothing error is larger than the discretizing error. With time increasing, the discretizing error increases, because the particle distribution becomes more and more irregular due to non-uniform flow in a heterogeneous field of hydraulic conductivity. Therefore, when solving the ADE using SPH and FPM, the SPH and FPM solutions may be similar in an early time, but FPM outperforms SPH when time increases. This is illustrated in the numerical examples discussed below.

### 3. Numerical investigation

The performance of SPH and FPM is investigated by using two numerical cases of two-dimensional solute transport modeling, with the focus on evaluating the effects of irregular particle distributions on accuracy of the SPH and FPM solutions. To simulate the particle distributions driven by “real” flow velocity, the irregular particle distributions are generated by advection process in heterogeneous

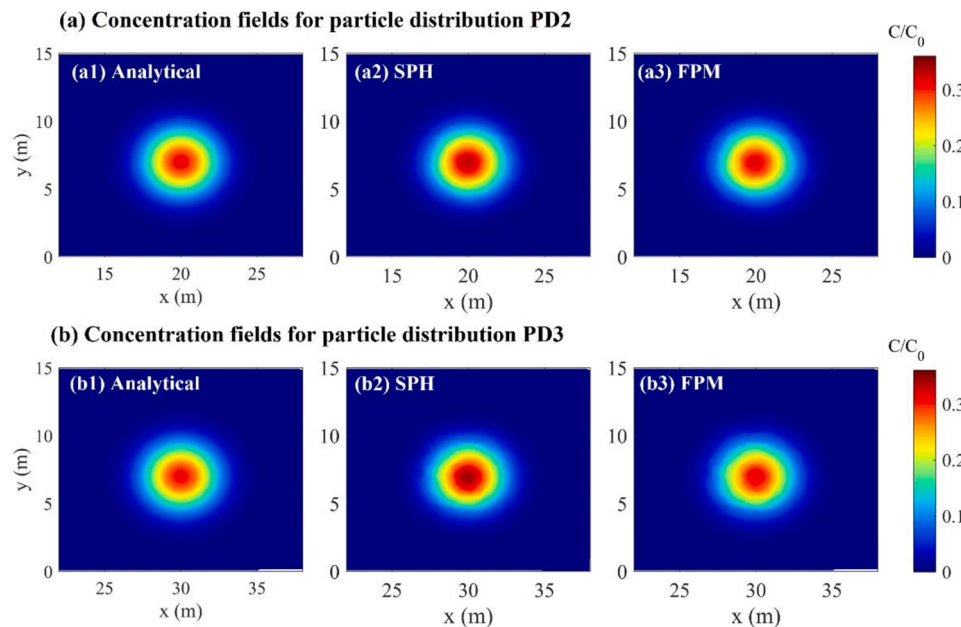


**Fig. 4.** (a) Two-dimensional plumes of the analytical, SPH, and FPM solutions of normalized concentration for particle distribution PD2. (b) Two-dimensional plumes of the analytical, SPH, and FPM solutions of normalized concentration for particle distribution PD3. The solutions are obtained at time  $t = 300$  h.

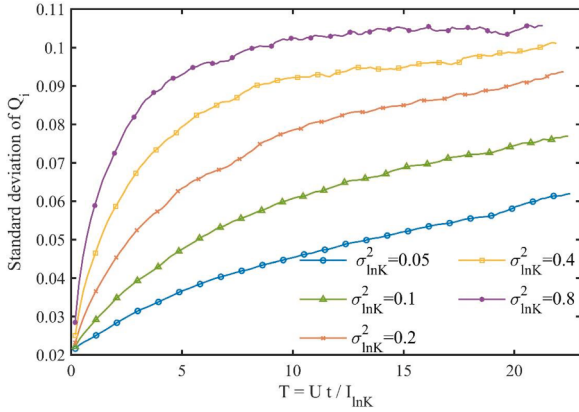


**Fig. 5.** Variation of the standard deviation of unity index,  $Q_i$ , as a function of dimensionless time ( $T = Ut / I_{lnK}$ ) for five heterogeneous fields of hydraulic conductivity with different  $\sigma_{lnK}^2$  values. where  $U$  is the mean seepage velocity in  $x$  direction, the integral scale,  $I_{lnK}$ , of heterogeneous hydraulic conductivity field is set as  $I_{lnK} = 8\Delta x = 1$  m.

hydraulic conductivity, and multiple variance values of log hydraulic conductivity are used for each case. To quantify the degree of irregular particle distributions, the unity index,  $Q$ , is used. For particle  $i$ , its unity index is defined as (Zhu et al., 2015)

$$Q_i = \sum_{j=1}^{N_b} \frac{m_j}{\rho_j} W_{ij} \quad (27)$$

which, according to Eq. (7), is the SPH approximation of a constant  $C_i = 1$ . For particle  $i$  with a complete support domain that is not intercepted by a boundary of the simulation domain, if the support domain has sufficient uniformly distributed neighbor particles, then  $Q_i$  equals 1; otherwise,  $Q_i$  follows a peaked distribution around 1 (Zhu et al., 2015). After  $Q_i$  is evaluated for all the particles, the standard deviation of  $Q_i$  is estimated and used to quantify the degree of particle irregularity. A larger standard deviation indicates a higher degree of particle irregularity. To analyze the errors of SPH and FPM solutions, the  $L_2$  norm of the errors relative to a reference solution (an analytical solution or a numerical solution of high accuracy) is calculated as

$$\text{error}_{L_2} = \| C_N / C_0 - C_R / C_0 \|_2 / N \quad (28)$$

where  $C_N / C_0$  is the numerical solution of normalized concentration ( $C_0$  being an initial concentration) given by SPH or FPM, and  $C_R / C_0$  is the reference solution of normalized concentration, and  $N$  is the total number of particles. In addition to the two numerical cases presented

below, an additional numerical case is considered in this study to validate our numerical codes of SPH and FPM. Description of the additional case is given in Text S1 and Figs. S1 – S5 of the supplementary information file.

### 3.1. Diffusive transport with irregular particle distributions

#### 3.1.1. Model setup and particle generation

This numerical case considers a diffusive transport problem with zero seepage velocity in a two-dimensional, confined domain with the size of 40 m × 15 m. The initial condition of the diffusive transport has an instantaneous Gaussian plume. The center of the Gaussian plume with the maximum concentration ( $C_0$ ) is placed at location  $(x_0, y_0)$ . For the two-dimensional diffusion problem, the analytical solution of the normalized solute concentration ( $C/C_0$ ) is (Zimmermann et al., 2001; Alvarado-Rodríguez et al., 2019; Herrera and Beckie, 2013)

$$\frac{C(\mathbf{x}, t)}{C_0} = \frac{w^2}{C_4} \exp\left(\frac{-(x-x_0)^2 A_1 - (y-y_0)^2 A_2 + 4(x-x_0)(y-y_0)A_3}{8t^2 C_2 + 4w^2 t C_3 + 2w^4}\right) \quad (29)$$

where  $A_1 = 2tD_{yy} + w^2$ ,  $A_2 = 2tD_{xx} + w^2$ ,  $A_3 = tD_{xy}$ ,  $C_2 = D_{xx}D_{yy} - D_{xy}^2$ ,  $C_3 = D_{xx} + D_{yy}$ ,  $C_4 = \sqrt{4t^2 C_2 + 2tw^2 C_3 + w^4}$ . The initial plume width is set as  $w = 1$  m, and the components of molecular diffusion coefficient are set as  $D_{xx} = D_{yy} = 1 \times 10^{-6}$  m<sup>2</sup>/s,  $D_{xy} = 0$ . The analytical solution is used to compare performance of SPH and FPM with uniformly and irregularly distributed particles in terms of solving the diffusion equation. For the SPH and FPM simulations, the total simulation time is set as  $t = 5,000\Delta t = 500$  h with the uniform time step  $\Delta t = 360$  s. This time step satisfies the relation of  $\Delta t \leq \epsilon h^2 / (D_{xx} + D_{yy})$  that has been used in literature (Herrera and Beckie, 2013; Herrera et al., 2009; Alvarado-Rodríguez et al., 2019), where  $\epsilon = 0.01$  is an empirical coefficient used in this study. The radius of the supporting domain of SPH and FPM is set as 2 h, and the smoothing length  $h$  is set as  $h = 1.5\Delta x = 0.1875$  m, where  $\Delta x = 0.125$  m is used for the MODFLOW simulation discussed below for generating three particle distributions.

For the diffusion transport problem, we conduct three numerical experiments with the plume center placed at locations (10 m, 7 m), (20 m, 7 m) and (30 m, 7 m), and each experiment has its own particle distribution generated by solving an advective transport problem in the same domain of diffusive transport using the predictor-corrector leap-frog time integration method discussed in Section 2.2. For the advective transport problem, a field of heterogeneous hydraulic conductivity is generated by using the “gstat” geostatistical package (Pebesma, 2004). It is assumed that the natural logarithm of the hydraulic conductivity,  $\ln K$ , follows the normal distribution with the mean of  $\langle \ln K \rangle = 1$  and the variance of  $\sigma_{\ln K}^2 = 0.1$ . An exponential covariance function with the

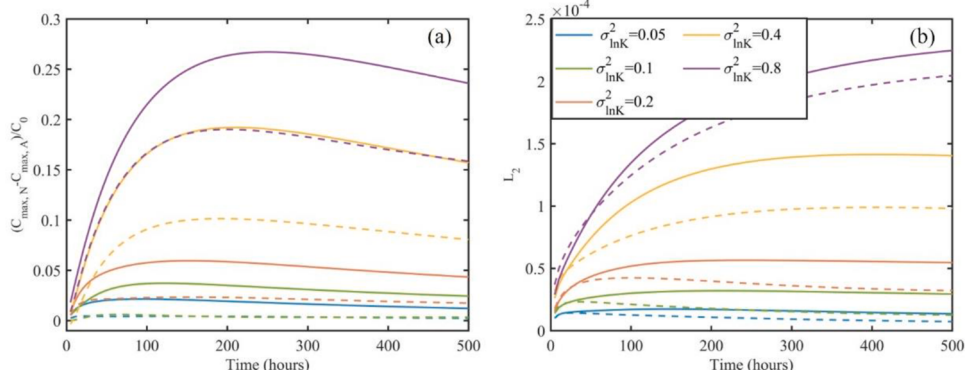


**Fig. 6.** (a) Temporal variation of the difference of maximum normalized concentration values,  $(C_{\max,N} - C_{\max,A})/C_0$ , between the SPH- and FPM-based numerical solution and the analytical solution for five  $\sigma_{\ln K}^2$  values. (b) Temporal variation of the  $L_2$  norm of the errors of the SPH and FPM solutions over the simulation domain. The solid and dashed lines are for the SPH and FPM solutions, respectively.

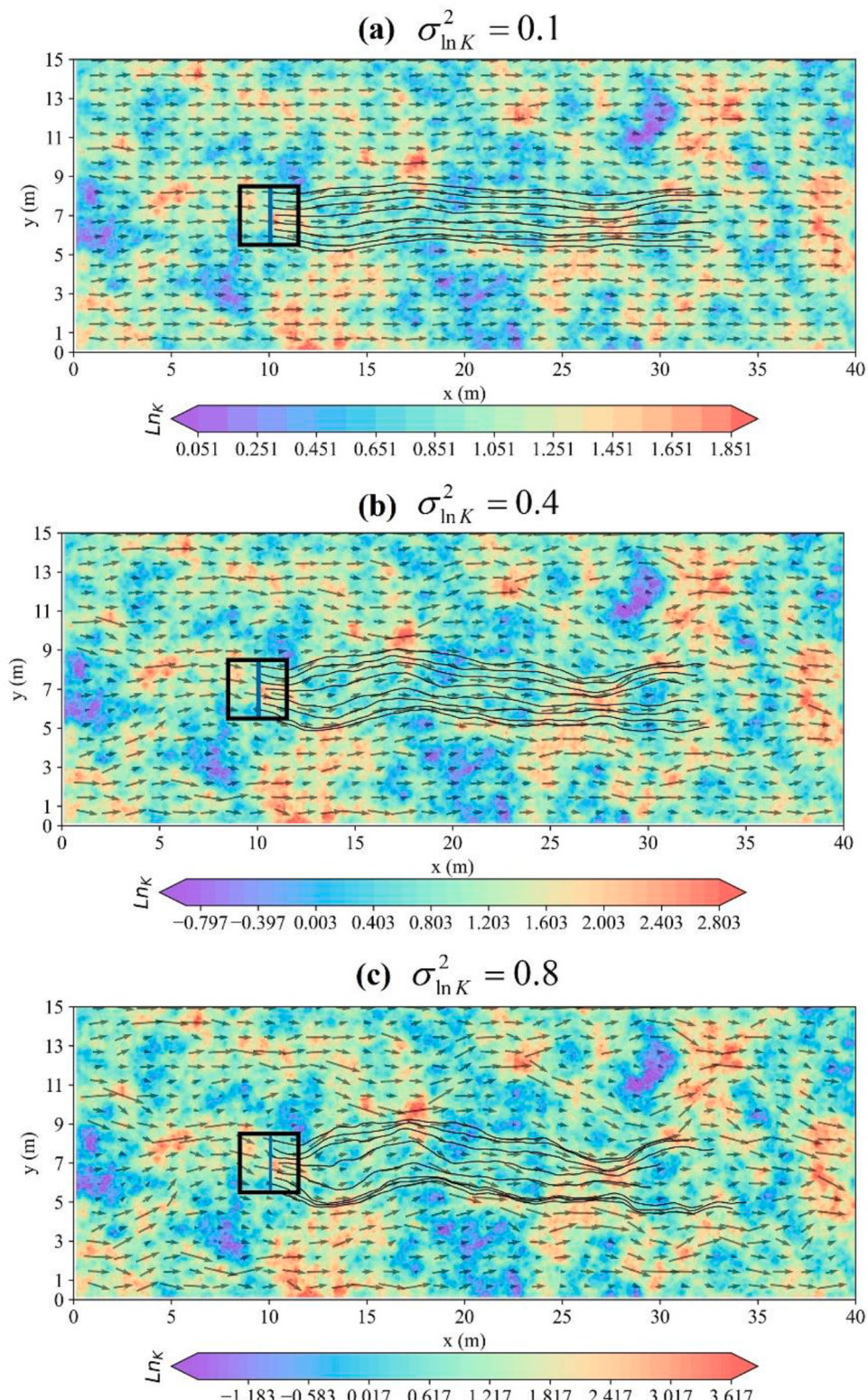


**Fig. 7.** Pathlines of particles that located at the center line of  $x = 10$  m within square contaminant plume for different heterogeneous fields of hydraulic conductivity field. (a) for  $\sigma_{\ln K}^2 = 0.1$ , (b) for  $\sigma_{\ln K}^2 = 0.4$ , and (c) for  $\sigma_{\ln K}^2 = 0.8$ . In the background, the log hydraulic conductivity field.

correlation length of  $I_{\ln K} = 1$  m is used to generate the heterogeneous hydraulic conductivity field. The flow direction is from a constant-head boundary at the left side to the constant-head boundary at the right side of the simulation domain; the top and bottom boundaries are set as no-flow boundaries. The groundwater flow is assumed to be steady, and MODFLOW 2000 (Harbaugh, 2000) is used to solve the flow problem.

The MODFLOW grid has 38,400 uniform blocks, and each block has the size of  $0.125 \text{ m} \times 0.125 \text{ m}$ . Seepage velocity is evaluated by using a constant porosity of 0.3 over the simulation domain.

Based on the MODFLOW-simulated flow field, three sets of particle distributions (one uniformly and two irregularly distributed) are generated. In the first set of particle distribution (PD1), particles are

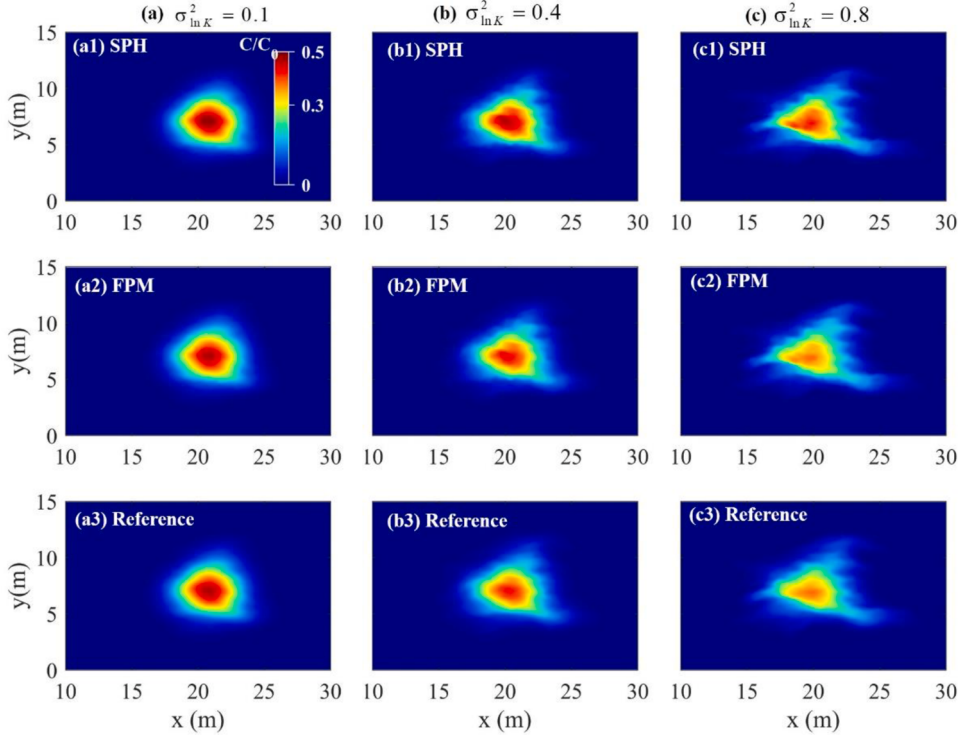


**Fig. 8.** Plumes of the SPH, FPM, and reference solutions at dimensionless time  $T = Ut/I_{\ln K} = 11.21, 10.95$ , and  $10.64$  used in the second numerical case for  $\sigma_{\ln K}^2 = 0.1, 0.4$ , and  $0.8$ , respectively.

uniformly placed at the MODFLOW block centers. The second set of particle distribution (PD2) is generated by first using PD1 as the initial particle distribution and then simulating advective transport of the particles using the predictor-corrector leapfrog time integration method with a constant timestep of  $\Delta t = 1800$  s. At the simulation time of  $t = 500\Delta t = 250$  h, the particle distribution is saved as PD2. Due to the non-uniform seepage velocity in the heterogeneous field of hydraulic conductivity, the particle positions of PD2 are irregular, with more particles in locations where pathlines converge and less particles in locations where the pathlines diverge. The third set of particle distribution (PD3) is generated in a same way of generating PD2 but using the particle distribution at time  $t = 1,000\Delta t = 500$  h. It should be noted that the computed flow field used for generating PD1 – PD3 is not completely divergent free. Since divergence of the flow field for an incompressible fluid is related to the temporal change of the fluid mass over a given volume, the generated particle distributions are affected by the divergence. This is a main drawback of the particle methods for simulating solute transport, and it also occurs for high-order finite volume and finite element methods. The three particle distributions are illustrated in Fig. 2 for an area of the size of  $10 \text{ m} \times 10 \text{ m}$  centered at the plume centers of  $(10 \text{ m}, 7 \text{ m})$ ,  $(20 \text{ m}, 7 \text{ m})$  and  $(30 \text{ m}, 7 \text{ m})$ . Fig. 2 shows that PD3 is more irregular than PD2, and PD1 is uniform. This is reflected in the standard deviation values of the unity index  $Q$ , and they are  $0.0201, 0.0628$ , and  $0.072$  for PD1 – PD3, respectively. The non-zero value of  $0.0201$  of PD1 is caused by incomplete support domains for particles whose distances to the boundaries are less than the radius of the support domains.

### 3.1.2. Results for $\sigma_{\ln K}^2 = 0.1$

Fig. 3 plots the three concentration profiles of the normalized concentration at simulation time  $t = 300$  h along the cross-section of  $y = 7 \text{ m}$  based on the analytical solution and the SPH and FPM solutions obtained using the three particle distributions. The normalized concentrations are based on the discrete particles. For the irregular distributed particles, since there are no particles exactly located at the line of  $y = 7 \text{ m}$ , the particles within the range of lines of  $y = 6.95 \text{ m}$  and  $y = 7.05 \text{ m}$  are used

to compare the two numerical solutions with the analytical solution. For particle distribution PD1 (Fig. 3(a)), since the particles are uniformly distributed, the SPH and FPM solutions are identical, and they coincide with the analytical solution. For particle distributions PD2 and PD3 with irregular particle distributions, the SPH solutions are larger than the analytical solutions at the centers the concentration profiles, as shown in Figs. 3(b) and 3(c). The errors of the SPH solution are significantly larger than those of the FPM solution, indicating that FPM outperforms SPH for the irregular particle distributions. The comparison of SPH, FPM, and deoupled FPM (FPM-D) solutions are shown in Fig. S6 of the supplementary information file, and the figure illustrates that the FPM and FPM-D solutions are visually identical.

Examining the two-dimensional plumes also indicates that FPM outperforms SPH. Fig. 4(a) plots the two-dimensional plumes at the simulation time of  $t = 300$  h given by the analytical solution and the SPH and FPM solutions obtained using PD2. Fig. 4(b) does the same for PD3. Both Figs. 4(a) and 3(b) show that SPH overestimates the maximum concentration at the plume centers. The overestimations are  $0.0192$  for PD2 and  $0.0411$  for PD3, which are  $6\%$  and  $13\%$  of the analytical solution of  $0.3164$ . This kind of overestimation was also reported in Alvarado-Rodríguez et al. (2019) and Avesani et al. (2015). While the overestimations also occur for FPM, they are substantially smaller, being  $2\%$  and  $1\%$  of the analytical solution for PD2 and PD3, respectively. The better performance of FPM is attributed to using the modified kernel gradient in Eq. (25) for FPM rather than the original kernel gradient in Eq. (15) for SPH. In SPH, the first-order derivatives of concentration in space are usually underestimated, because the integrations of  $(x_i - x_j)\nabla_{i,x}W_{ij}$  over the support domain are usually less than 1 (e.g.,  $0.8060$  in Fig. 1(a4)) for a limited number of irregularly distributed particles. As a result, the time rate change of concentration in Eq. (25) is underestimated, and this leads to the overestimation of the normalized concentration at the plume centers (Fig. 3) and an underestimation away from the plume centers. An illustration of the underestimation problem is given in Fig. S3 of the supplementary information file. The problems of overestimation and underestimation are alleviated by FPM because of

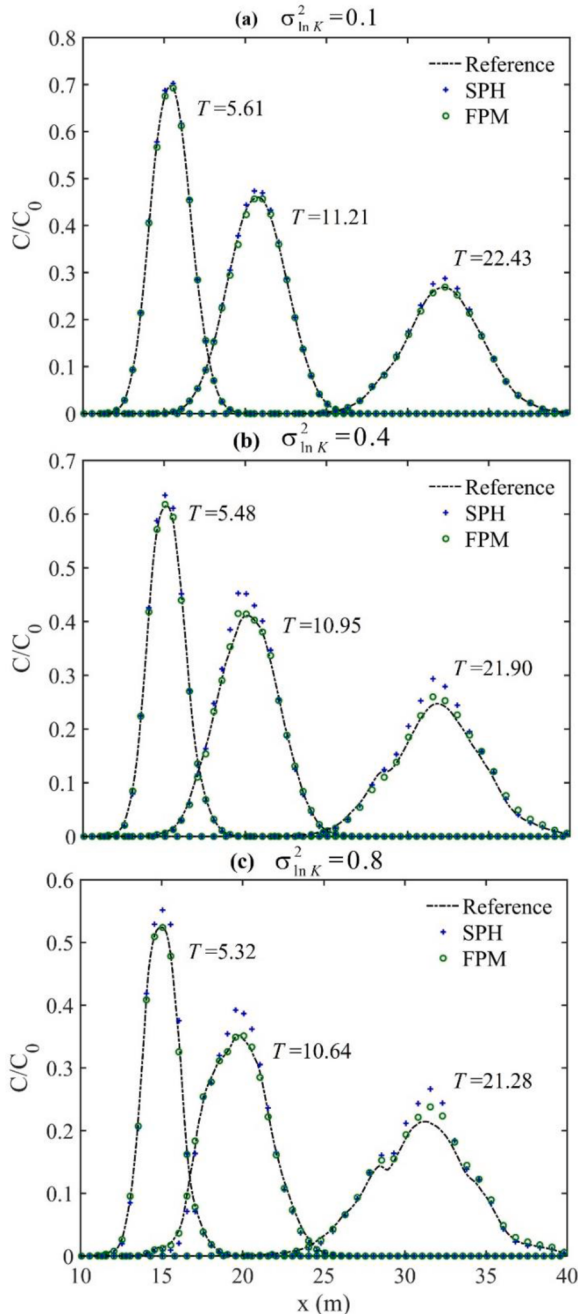


**Fig. 9.** Profiles of reference, SPH, and FPM solutions of normalized concentration ( $C/C_0$ ) along the line of  $y = 7.5$  m for three different simulation dimensionless times for three values of  $\sigma_{\ln K}^2$ . (a) for  $\sigma_{\ln K}^2 = 0.1$ , (b) for  $\sigma_{\ln K}^2 = 0.4$ , and (c) for  $\sigma_{\ln K}^2 = 0.8$ .

the use of the modified kernel gradients. Fig.S4 of supplementary information file plots the convergence rates based on the relative  $L_2$  norm of the numerical solutions. The figure indicates that FPM converges to the reference solution at a faster rate than SPH does. The high accuracy of FPM is attributed to the correction made to kernel gradient as discussed before. The correction however makes FPM computationally more expensive than SPH. Take as an example the diffusive transport problem with the irregular particle distribution of PD3 with  $\sigma_{\ln K}^2 = 0.1$ . For a computer with Intel(R) Core (TM) i7-8550 U CPU of 1.99 GHz, the CPU time averaged over 10 repeated runs is 18.719 s and 19.678 s for SPH and FPM, respectively.

### 3.1.3. Results for different $\sigma_{\ln K}^2$ values

In addition to  $\sigma_{\ln K}^2 = 0.1$ , this study also considers four additional fields of heterogeneous hydraulic conductivity with  $\sigma_{\ln K}^2 = 0.05, 0.2, 0.4$ , and  $0.8$  to further evaluate SPH and FPM performance with an increasing level of particle irregularity caused by the increasing level of heterogeneity. For each  $\sigma_{\ln K}^2$  value, a particle distribution is generated in the same way of generating PD3 by solving the advective transport problem and saving the particle distribution at time  $t = 1,000\Delta t = 500$  h. For the particle distributions of the five  $\sigma_{\ln K}^2$  values, the standard deviation of the unit index  $Q_i$  is evaluated, and the standard deviation values are plotted in Fig. 5. The figure also plots the standard deviation values for multiple particle distributions generated at different dimensionless times,  $T = Ut/I_{\ln K}$ , for each  $\sigma_{\ln K}^2$  value, where  $U$  is the mean seepage velocity in  $x$  direction. The figure shows that, for each  $\sigma_{\ln K}^2$  value, the irregularity of the particle distributions increases with time due to particle movement. When  $\sigma_{\ln K}^2$  increases, heterogeneity of hydraulic conductivity increases, and irregularity of the particle distributions increases accordingly. Fig. S7 of the supplementary information file illustrates three particle distributions generated for each  $\sigma_{\ln K}^2$  value. The particle irregularity for  $\sigma_{\ln K}^2 = 0.8$  is already large enough, as indicated by Fig. S9 that plots the standard deviation of the unit index  $Q_i$  for  $\sigma_{\ln K}^2 = 0.2, 0.4, 0.8, 2.0, 4.0$ , and  $8.0$ .

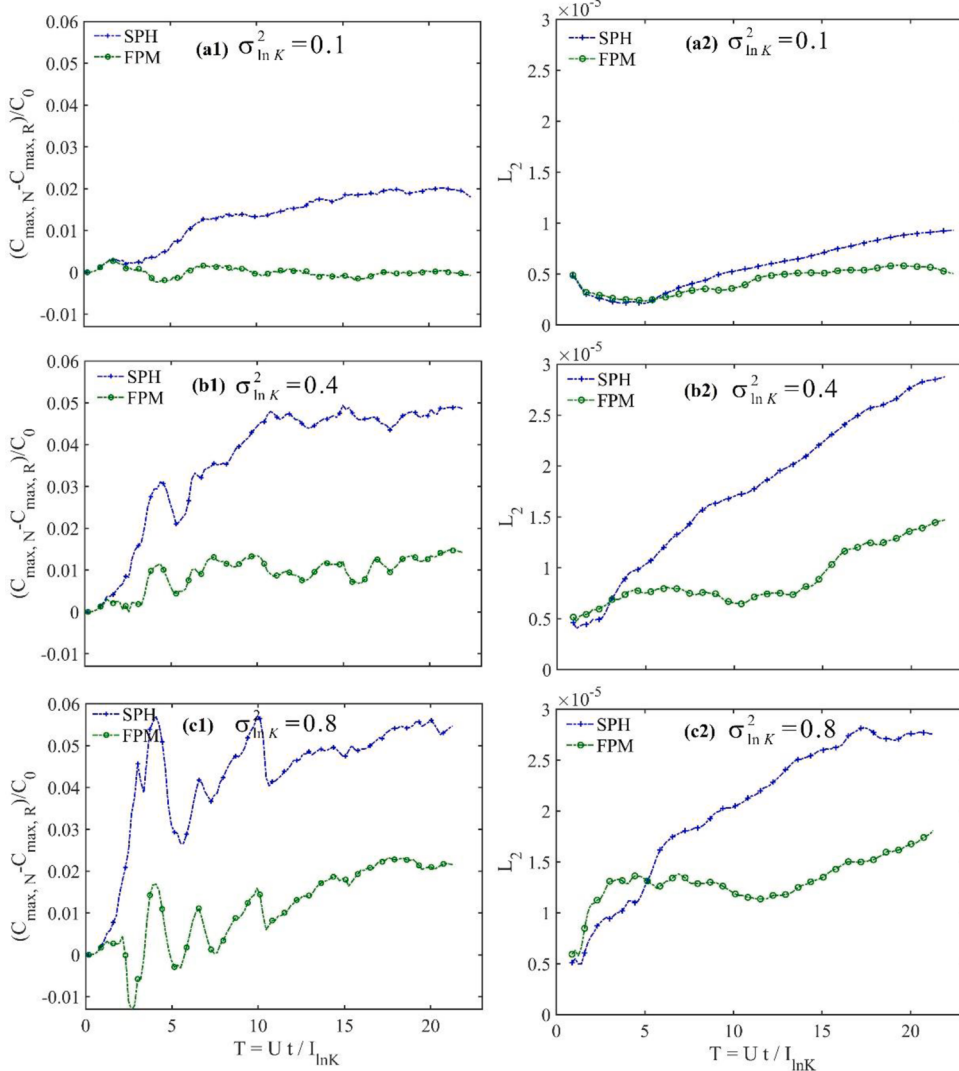
The five particle distributions generated for time  $t = 1,000\Delta t = 500$  h are used for the third experiment discussed above with the initial plume center placed at (30 m, 7 m), and the accuracy of SPH and FPM is evaluated for the maximum normalized concentration at the plume center and over the entire simulation domain. If a particle distribution has high irregularity, its matrix  $M$  may be ill-conditioned or even singular, and the system equation of  $M\nabla_i^M W_{ij} = \nabla_i W_{ij}$  cannot be solved. To resolve this problem, the decoupled FPM discussed in Section 2.3 is used. After the diffusive transport problem is solved by using SPH and FPM (coupled or decoupled), accuracy of the SPH and FPM numerical solutions is evaluated by evaluating the difference of the maximum normalized concentration (i.e.,  $C_{max,N}/C_0 - C_{max,A}/C_0$  or equivalently  $(C_{max,N} - C_{max,A})/C_0$ ) between the numerical solutions and the analytical solution of Eq. (29). The differences are positive for both SPH and FPM, indicating the overestimation problem discussed above. The differences are plotted with time in Fig. 6(a) for the five  $\sigma_{\ln K}^2$  values. The figure shows that, while accuracy of both SPH and FPM deteriorates when  $\sigma_{\ln K}^2$  increases, FPM is more accurate than SPH for each  $\sigma_{\ln K}^2$  over the entire simulation time. Accuracy of SPH and FPM is also evaluated for the entire domain by using the  $L_2$  norm of numerical error defined in Eq. (28), and the variation of the  $L_2$  norm with time is plotted in Fig. 6(b) for the five  $\sigma_{\ln K}^2$  values. The figure shows that, while the  $L_2$  norms of both SPH and FPM increases when  $\sigma_{\ln K}^2$  increases, the  $L_2$  norm of FPM is smaller than that of SPH for each  $\sigma_{\ln K}^2$  over the entire simulation time.

Fig. 6 shows that the temporal patterns of the SPH and FPM solutions are similar. It is further noted that the temporal pattern of Fig. 6(a) for the difference of maximum normalized concentration is different from the temporal pattern of Fig. 6(b) for the  $L_2$  norm, especially for large  $\sigma_{\ln K}^2$  values. Taking  $\sigma_{\ln K}^2 = 0.8$  as an example, the difference increases until about 200 h and then decreases, where the  $L_2$  norm keeps increasing. This is due to the problem of overestimating the normalized concentration at the plume center as discussed in Section 3.1.2. The overestimation may accumulate over time until the plume spreads out over the simulation domain. For the  $L_2$  norm calculated for the entire domain, it accounts for both overestimation and underestimation over the simulation domain, and thus increases with time.

## 3.2. Advection and dispersion in heterogeneous flow field

### 3.2.1. Model setup

This numerical case is generally similar to the first numerical case described above, and the differences between the two cases are



**Fig. 10.** (a1) Temporal variation of the difference of maximum normalized concentration,  $(C_{\max,N} - C_{\max,R})/C_0$ , between the SPH- and the FPM-based numerical solutions and the reference solution, and (a2)  $L^2$  norm of the errors of the SPH and FPM solutions over the simulation domain in a heterogeneous field of hydraulic conductivity with  $\sigma_{\ln K}^2 = 0.1$ . Plots (b1) – (b2) and plots (c1) – (c2) are for the heterogeneous fields of hydraulic conductivity with  $\sigma_{\ln K}^2 = 0.4$  and  $\sigma_{\ln K}^2 = 0.8$ , respectively.

described here. Different from the first numerical case, this numerical case considers both advection and dispersion, and is thus more realistic. In this numerical case, the flow problem is the same as that of the first numerical case described in Section 3.1. The initial condition of this numerical case has an instantaneous concentration  $C_0$  that is a constant over a square with the size of  $L = 3$  m centered at the location of (10 m, 7 m). The total simulation time is set as  $t = 1,200\Delta t$  with a uniform time step of  $\Delta t = 1800$  s. We consider three variance values of log hydraulic conductivity, i.e.,  $\sigma_{\ln K}^2 = 0.1$ , 0.4, and 0.8. For each  $\sigma_{\ln K}^2$ , the initial particle distribution at  $t = 0$  is uniform, and the particles are placed at the center of the MODFLOW blocks. When the particles move with the flow, the particle distribution becomes more and more irregular. For each  $\sigma_{\ln K}^2$ , the smoothing length is set as  $h = 1.5\Delta x = 0.1875$  m when implementing SPH and FPM.

Since there is no analytical solution for this numerical case, to evaluate the performance of SPH and FPM, a reference solution is obtained by using SPH with a smaller particle spacing of  $\Delta x = \Delta y = 0.03125$  m and smoothing length of  $h = 0.3$  m. These values are chosen based on the general principles discussed in Section 2.4 that accurate SPH solutions can be obtained by using a smoothing length,  $h$ , to have a large number of particles within a support domain (Zhu et al., 2015; Herrera et al., 2009). Figs. S10 and S11 of the supplementary information file show the effects of  $\Delta x$  and  $h$ , respectively, on the SPH based reference solution, and Text S2 of the supplementary information file

explains the reason of choosing  $\Delta x = 0.03125$  m and  $h = 0.3$  m to obtain the reference solution. Because the particles used for the reference solution are different from those used for implementing SPH and FPM in this numerical case, to compare the FPM and SPH solutions with the reference solution, the three solutions are interpolated to the MODFLOW grid that has uniform blocks, each has the size of  $\Delta x = \Delta y = 0.125$  m. The interpolation is conducted by using the MATLAB scatter interpolation function, *ScatteredInterpolant*, with the “natural” option for the function. The interpolation is only used for comparing the SPH and FPM solutions with the reference solution, not for implementing the SPH and FPM methods.

### 3.2.2. Results

Fig. 7 plots the pathlines of the particles that are placed along the line of  $x = 10$  m within the square of the initial plume for heterogeneous fields of hydraulic conductivity with three  $\sigma_{\ln K}^2$  values. The pathlines for the case of  $\sigma_{\ln K}^2 = 0.1$  are significantly more uniform than those for the cases of  $\sigma_{\ln K}^2 = 0.4$  and  $\sigma_{\ln K}^2 = 0.8$ . For the latter two cases, the converging flow zones have more particles than the diverging flow zones. Fig. 8 plots the concentration plumes of SPH, FPM and reference solutions at dimensionless time  $T = 11.21$ , 10.95, and 10.64 for three  $\sigma_{\ln K}^2$  values of 0.1, 0.4, and 0.8, respectively. In Figs. 8(a1 – a3) for  $\sigma_{\ln K}^2 = 0.1$ , comparing with the reference solution, SPH overestimates the maximum normalized concentration by about 3% (the reference

solution is 0.4728 and the SPH solution is 0.4872), whereas FPM overestimate the maximum normalized solution by 0.2% (the FPM solution is 0.4729). For  $\sigma_{lnK}^2 = 0.4$ , the reference solution is 0.4248, and the SPH and FPM solutions are 0.4723 and 0.4333, respectively. The overestimation increases to 11% and 2% for SPH and FPM, respectively. For  $\sigma_{lnK}^2 = 0.8$ , the reference solution is 0.3788, and the SPH and FPM solutions are 0.4191 and 0.3859, respectively. The overestimation remains as 11% and 2% for SPH and FPM, respectively. These results indicate that the FPM solutions are more accurate than the SPH solutions for all the three levels of particle irregularity.

Figs. 9(a) – 9(c) plot the profiles of the reference, SPH, and FPM solutions along  $y = 7.5$  m at different simulation dimensionless times for three  $\sigma_{lnK}^2$  values of 0.1, 0.4, and 0.8. The profiles along  $y = 7.5$  m are chosen because, while the initial plume center is located at (10 m, 7 m), the solute plume moves roughly along the line of  $y = 7.5$  due to non-uniform velocity, as shown in Figs. 8(c1) – 8(c3). Fig. 9(a) shows that, for  $\sigma_{lnK}^2 = 0.1$ , the SPH and FPM solutions are visually identical to the reference solution at early time of  $T = 5.61$ ; when time increases, the SPH solution deviates from the reference solutions, but the FPM solution is still visually identical to the reference solution. This is not surprising given that the initial particle distribution is uniform and that irregularity of the particle distribution is relatively small for  $\sigma_{lnK}^2 = 0.1$ . When  $\sigma_{lnK}^2$  increases to 0.4 and 0.8, Figs. 9(b) and 9(c) show that the SPH and FPM solutions become less accurate. The SPH solutions are different from the reference solutions even at the early time of  $T = 5.48$  for  $\sigma_{lnK}^2 = 0.4$  and  $T = 5.32$  for  $\sigma_{lnK}^2 = 0.8$ ; the FPM solutions are still accurate at the early time, but becomes different from the reference solutions when time increases. Figs. 9(a), 9(b) and 9(c) consistently indicate that the FPM solutions are more accurate than the SPH solutions for all the three simulation times and for all the three  $\sigma_{lnK}^2$  values that generate different levels of particle irregularity.

Figs. 10(a1) – 10(c1) plot the differences of maximum normalized concentration calculated over the entire simulation period for  $\sigma_{lnK}^2 = 0.1$ , 0.4, and 0.8, respectively. The FPM solutions are more accurate than the SPH solutions, because FPM simulates more dispersion with the modified kernel gradients and thus alleviates the SPH underestimation of time rate change of concentration. The results are consistent with those of the diffusive transport problem discussed in Section 3.1.2. Figs. 10(a2) – 10(c2) do the same for the  $L_2$  norm calculated for the entire simulation domain. These figures lead to a conclusion that FPM is more accurate than SPH over the entire simulation period for all the three  $\sigma_{lnK}^2$  values that generate different levels of particle irregularity. It is noted that the  $L_2$  norm of FPM is larger than that of SPH in the early simulation time ( $t < 140$  h), which may be resulted from the effect the numerical error introduced by the correction matrix in FPM. The numerical error may be relatively large at early time, when accumulative discretizing error caused by irregular particle distribution is small with small change in concentration. An in-depth understanding of the numerical error is warranted in a future study.

Figs. 9 and 10 indicate that accuracy of SPH and FPM solutions is affected by simulation time and heterogeneity of hydraulic conductivity. As discussed in Section 3.1.3 for Fig. 5, the both factors are sources of particle irregularity for heterogeneous hydraulic conductivity, because uniformly distributed particles become more irregular over time and when heterogeneity of hydraulic conductivity increases. When particle irregularity increases, the errors of the SPH-based ADE solutions accumulate over time, and become large for larger  $\sigma_{lnK}^2$  values. The FPM-based solutions are more accurate than the SPH-based solutions because of using the modified kernel gradient given in Eq. (24), although the FPM-based solutions also become less accurate when time increases and/or hydraulic conductivity becomes more heterogeneous.

#### 4. Conclusions

To the best of our knowledge, this study is the first attempt of using FPM to solve ADE for groundwater solute transport modeling. FPM is developed as an improvement of SPH to obtain more accurate numerical solutions when particle distributions become irregular. In groundwater modeling, initially uniformly distributed particles become irregularly distributed, when the particles move with groundwater flow in a heterogeneous field of hydraulic conductivity, with more (less) particles flowing to locations where flow pathlines converge (diverge). For the irregularly distributed particles, we demonstrate that the unity and symmetric properties of a SPH kernel function and the anti-symmetric property of the kernel gradient may not be satisfied. The unsatisfied anti-symmetric property directly affects accuracy of SPH-based solutions. The accuracy is improved by FPM by using the modified kernel gradient that is based on the SPH kernel function and its first-order derivatives. This makes the implementation of FPM straightforward based on existing SPH codes.

Accuracy of the SPH- and FPM-based ADE solutions is examined in two numerical cases with irregularly distributed particles. The first case considers diffusion only, and has an analytical solution that is used as a reference solution to evaluate accuracy of the SPH and FPM solutions. The second case considers both advection and dispersion, and uses a numerical solution (obtained using SPH with a large number of particles and a large smoothing length to reduce computational errors) as a reference solution. Accuracy of the SPH and FPM solutions is evaluated with respect to the difference of maximum normalized concentration calculated at the plume center and the  $L_2$  norm calculated for the simulation domain. For the limited number of numerical experiments analyzed in this study, FPM outperforms SPH to yield more accurate solutions. In particular, the overestimation problem of SPH at the plume centers is substantially alleviated by using FPM, which is attributed to using the modified kernel gradient in FPM.

The numerical errors of the SPH and FPM solutions increase, if particle distributions become more irregular when simulation time increases and/or hydraulic conductivity becomes more heterogeneous. It is found in this study that the FPM solutions are substantially more accurate than the SPH solutions, indicating that FPM should be used when simulation time is long and/or heterogeneity of hydraulic conductivity is relatively high. For highly heterogeneous hydraulic conductivity, a further improvement of FPM is needed, which is however beyond the scope of this study. This study uses a fixed smoothing length and thus the same number of particles for all numerical simulations. Impacts of the smoothing length and the number of particles on FPM solutions is warranted in a future study. In addition, this study only compares FPM with the standard SPH, and a comparison between FPM and improved SPH methods is also warranted in a future study.

#### CRediT authorship contribution statement

**Tian Jiao:** Conceptualization, Investigation, Methodology, Writing – original draft. **Ming Ye:** Conceptualization, Methodology, Supervision, Writing – review & editing. **Menggui Jin:** Conceptualization, Supervision, Writing – review & editing. **Jing Yang:** Writing – review & editing.

#### Declaration of Competing Interest

The authors declare that they have no known competing financial interests or personal relationships that could have appeared to influence the work reported in this paper.

#### Acknowledgments

We thank the three anonymous reviewers for their constructive and insightful suggestions that have improved the content of the manuscript. This study was supported by the National Natural Science Foundation of

China (No. 41877192). The first author was supported by the Fundamental Research Funds for National Universities to the China University of Geosciences University of Geosciences (Wuhan) for her research at the Florida State University. The second author was supported by NSF Grant EAR-1552329.

## Supplementary materials

Supplementary material associated with this article can be found, in the online version, at doi:[10.1016/j.advwatres.2021.104043](https://doi.org/10.1016/j.advwatres.2021.104043).

## References

- Alvarado-Rodríguez, C.E., Sigalotti, L.D.G., Klapp, J., 2019. Anisotropic dispersion with a consistent smoothed particle hydrodynamics scheme. *Adv. Water Resour.* 131, 103374 doi:[10.1016/j.advwatres.2019.07.004](https://doi.org/10.1016/j.advwatres.2019.07.004).
- Avesani, D., Dumbser, M., Chiogna, G., Bellin, A., 2017. An alternative smooth particle hydrodynamics formulation to simulate chemotaxis in porous media. *J. Math. Biol.* 74, 1037–1058, 10.1007/s00285-016-1049-6.
- Avesani, D., Dumbser, M., Vacondo, R., Righetti, M., 2021. An alternative SPH formulation: ADER-WENO-SPH. *Comput. Methods Appl. Mech. Eng.* 382 doi.org/10.1016/j.cma.2021.113871.
- Avesani, D., Herrera, P., Chiogna, G., Bellin, A., Dumbser, M., 2015. Smooth Particle Hydrodynamics with nonlinear Moving-Least-Squares WENO reconstruction to model anisotropic dispersion in porous media. *Adv. Water Resour.* 80, 43–59, 10.1016/j.advwatres.2015.03.007.
- Batra, R.C., Zhang, G.M., 2004. Analysis of adiabatic shear bands in elasto-thermo-viscoplastic materials by modified smoothed-particle hydrodynamics (MSPH) method. *J. Comput. Phys.* 201 (1), 172–190, 10.1016/j.jcp.2004.05.007.
- Benson, D.A., Tomás, A., Diogo, B., Engdahl, N., Henri, C.V., Fernández-García, D., 2017. A comparison of Eulerian and Lagrangian transport and non-linear reaction algorithms. *Adv. Water Resour.* 99, 15–37, 10.1016/j.advwatres.2016.11.003.
- Boso, F., Bellin, A., Dumbser, M., 2013. Numerical simulations of solute transport in highly heterogeneous formations: a comparison of alternative numerical schemes. *Adv. Water Resour.* 52, 178–189, 10.1016/j.advwatres.2012.08.006.
- Chaniotis, A.K., Frouzakis, C.E., Lee, J.C., Tomboulides, A.G., Poulikakos, D., Boulouchos, K., 2003. Remeshed smoothed particle hydrodynamics for the simulation of laminar chemically reactive flows. *J. Comput. Phys.* 191 (1), 1–17, 10.1016/s0021-9910(03)00302-4.
- Chen, J.K., Beraun, J.E., 2000. A generalized smoothed particle hydrodynamics method for nonlinear dynamic problems. *Comput. Methods Appl. Mech. Eng.* 190, 225–239, 10.1016/s0045-7825(99)00422-3.
- Chen, J.K., Beraun, J.E., Carney, T.C., 1999. A corrective smoothed particle method for boundary value problems in heat conduction. *Internat. J. Numer. Meth. Engrg.* 46, 231–252 doi.org/10.1002/(SICI)1097-0207(19990920)46:2<231::AID-NME672>3.0.CO;2-K.
- Cleary, P.W., Monaghan, J.J., 1999. Conduction modelling using smoothed particle hydrodynamics. *J. Comput. Phys.* 148 (1), 227–264 doi:[10.1006/jcph.1998.6118](https://doi.org/10.1006/jcph.1998.6118).
- de Barros, F.P.J., Fiori, A., Boso, F., Bellin, A., 2015. A theoretical framework for modeling dilution enhancement of non-reactive solutes in heterogeneous porous media. *J. Contam. Hydrol.* 175–176, 72–83. doi:[10.1016/j.jconhyd.2015.01.004](https://doi.org/10.1016/j.jconhyd.2015.01.004).
- Dehnen, W., Aly, H., 2012. Improving convergence in smoothed particle hydrodynamics without pairing instability. *Mon. Not. R. Astron. Soc.* 425 (2), 1068–1082 https://doi.org/10.1111/j.1365-2966.2012.21439.x.
- Espanol, P., Revenga, M., 2003. Smoothed dissipative particle dynamics. *Phys. Rev. E.* 67, 026705, 10.1103/PhysRevE.67.026705.
- Harbaugh, A., 2000. MODFLOW-2000, the US Geological Survey Modular Groundwater Model: user guide to modularization concepts and the ground-water flow process. US Geol. Survey.
- Herrera, P.A., Beckie, R.D., 2013. An assessment of particle methods for approximating anisotropic dispersion. *Int. J. Numer. Meth. Fluids.* 71 (5), 634–651, 10.1002/fld.3676.
- Herrera, P.A., Cortínez, J.M., Valocchi, A.J., 2017. Lagrangian scheme to model subgrid-scale mixing and spreading in heterogeneous porous media. *Water Resour. Res.* 53 (4), 3302–3318, 10.1002/2016wr019994.
- Herrera, P.A., Massabó, M., Beckie, R.D., 2009. A meshless method to simulate solute transport in heterogeneous porous media. *Adv. Water Resour.* 32 (3), 413–429, 10.1016/j.advwatres.2008.12.005.
- Herrera, P.A., Valocchi, A.J., Beckie, R.D., 2010. A multidimensional streamline-based method to simulate reactive solute transport in heterogeneous porous media. *Adv. Water Resour.* 33 (7), 711–727, 10.1016/j.advwatres.2010.03.001.
- Huang, C., Zhang, D.H., Si, Y.L., Shi, Y.X., Lin, Y.G., 2018. Coupled finite particle method for simulations of wave and structure interaction. *Coast Eng. J.* 140, 147–160, 10.1016/j.coastaleng.2018.07.003.
- Konikow, L.F., 2011. The secret to successful solute-transport modeling. *Groundwater* 49 (2), 144–159, 10.1111/j.1745-6584.2010.00764.
- Liu, G.R., Liu, M.B., 2003. Smoothed Particle Hydrodynamics: A Meshfree Particle Method. World Scientific, Singapore.
- Liu, M.B., Liu, G.R., 2006. Restoring particle consistency in smoothed particle hydrodynamics. *Appl. Numer. Math.* 56 (1), 19–36, 10.1016/j.apnum.2005.02.012.
- Liu, M.B., Liu, G.R., 2010. Smoothed Particle Hydrodynamics (SPH): an overview and recent developments. *Arch. Comput. Methods Eng.* 17 (1), 25–76, 10.1007/s11831-010-9040-7.
- Liu, M.B., Xie, W.P., Liu, G.R., 2005. Modeling incompressible flows using a finite particle method. *Appl. Math. Model.* 29 (12), 1252–1270, 10.1016/j.apm.2005.05.003.
- Monaghan, J.J., 2005. Smoothed particle hydrodynamics. *Rep. Prog. Phys.* 68 (8), 1703–1759, 10.1088/0034-4885/68/8/r01.
- Montanino, A., Asprone, D., Reali, A., Auricchio, F., 2017. Modified finite particle methods for Stokes problems. *Comput. Part. Mech.* 5 (2), 141–160, 10.1007/s40571-017-0159-2.
- Pebesma, E.J., 2004. Multivariable geostatistics in S: the gstat package. *Comput. Geosci.* 30 (7), 683–691, 10.1016/j.cageo.2004.03.012.
- Radu, F.A., Suciu, N., Hoffmann, J., Vogel, A., Kolditz, O., Park, C.-H., Attinger, S., 2011. Accuracy of numerical simulations of contaminant transport in heterogeneous aquifers: a comparative study. *Adv. Water Resour.* 34 (1), 47–61, 10.1016/j.advwatres.2010.09.012.
- Sigalotti, L.D.G., Klapp, J., Rendón, O., Vargas, C.A., Peña Polo, F., 2016. On the kernel and particle consistency in smoothed particle hydrodynamics. *Appl. Numer. Math.* 108, 242–255, 10.1016/j.apnum.2016.05.007. Appl.
- Sole-Mari, G., Fernández-García, D., 2018. Lagrangian modeling of reactive transport in heterogeneous porous media with an automatic locally adaptive particle support volume. *Water Resour. Res.* 54 (10), 8309–8331, 10.1029/2018wr023033.
- Tartakovsky, A.M., 2010. Lagrangian simulations of unstable gravity-driven flow of fluids with variable density in randomly heterogeneous porous media. *Stoch. Environ. Res. Risk Assess.* 24 (7), 993–1002, 10.1007/s00477-010-0402-3.
- Tartakovsky, A.M., Meakin, P., 2005. A smoothed particle hydrodynamics model for miscible flow in three-dimensional fractures and the two-dimensional Rayleigh–Taylor instability. *J. Comput. Phys.* 207 (2), 610–624, 10.1016/j.jcp.2005.02.001.
- Tartakovsky, A.M., Meakin, P., Scheibe, T.D., Eichler West, R.M., 2007a. Simulations of reactive transport and precipitation with smoothed particle hydrodynamics. *J. Comput. Phys.* 222 (2), 654–672, 10.1016/j.jcp.2006.08.013.
- Tartakovsky, A.M., Meakin, P., Scheibe, T.D., Wood, B.D., 2007b. A smoothed particle hydrodynamics model for reactive transport and mineral precipitation in porous and fractured porous media. *Water Resour. Res.* 43 (5), W0543710.1029/2005wr004770.
- Tartakovsky, A.M., Tartakovsky, G.D., Scheibe, T.D., 2009. Effects of incomplete mixing on multicomponent reactive transport. *Adv. Water Resour.* 32 (11), 1674–1679, 10.1016/j.advwatres.2009.08.012.
- Werth, C.J., Cirpka, O.A., Grathwohl, P., 2006. Enhanced mixing and reaction through flow focusing in heterogeneous porous media. *Water Resour. Res.* 42 (12), W12414. doi.org/10.1029/2005WR004511.
- Xu, X., Deng, X.L., 2016. An improved weakly compressible SPH method for simulating free surface flows of viscous and viscoelastic fluids. *Comput. Phys. Comm.* 201, 43–62, 10.1016/j.cpc.2015.12.016.
- Yildiz, M., Rook, R.A., Suleiman, A., 2009. SPH with the multiple boundary tangent method. *Int. J. Numer. Meth. Eng.* 77, 1416–1438, 10.1002/nme.2458.
- Zhang, G.M., Batra, R.C., 2004. Modified smoothed particle hydrodynamics method and its application to transient problems. *Comput. Mech.* 34 (2), 137–146, 10.1007/s00466-004-0561-5.
- Zhang, G.M., Batra, R.C., 2008. Symmetric smoothed particle hydrodynamics (SSPH) method and its application to elastic problems. *Comput. Mech.* 43 (3), 321–340, 10.1007/s00466-008-0308-9.
- Zhang, Z.L., Liu, M.B., 2018. A decoupled finite particle method for modeling incompressible flows with free surfaces. *Appl. Math. Model.* 60, 606–633, 10.1016/j.apm.2018.03.043.
- Zhang, Z.L., Walayat, K., Chang, J.Z., Liu, M.B., 2018. Meshfree modeling of a fluid-particle two-phase flow with an improved SPH method. *Int. J. Numer. Methods Eng.* 116 (8), 530–569, 10.1002/nme.5935.
- Zhang, Z.L., Walayat, K., Huang, C., Chang, J.Z., Liu, M.B., 2019. A finite particle method with particle shifting technique for modeling particulate flows with thermal convection. *Int. J. Heat Mass Transf.* 128, 1245–1262, 10.1016/j.ijheatmasstransfer.2018.09.074.
- Zheng, C., Wang, P.P., 1999. MT3DMS. A modular three-dimensional multispecies transport model for simulation of advection, dispersion, and chemical reactions of contaminants in groundwater systems; documentation and user's guide. ed. U.A.C.O. Engineers.
- Zhou, Z.K., Shi, L.S., Zha, Y.Y., 2020. Effects of local transverse dispersion on macro-scale coefficients of oxygen-limited biodegradation in a stratified formation. *J. Contam. Hydrol.* 228, 103580. doi.org/10.1016/j.jconhyd.2019.103580.
- Zhu, Q., Hernquist, L., Li, Y., 2015. Numerical convergence in smoothed particle hydrodynamics. *Astrophys. J.* 800, 6, 10.1088/0004-637x/800/1.
- Zhu, Y., Fox, P.J., 2001. Smoothed particle hydrodynamics model for diffusion through porous media. *Transp. Porous Media* 43 (3), 441–471 https://doi.org/10.1023/A:1010769915901.
- Zimmermann, S., Koumoutsakos, P., Kinzelbach, W., 2001. Simulation of pollutant transport using a particle method. *J. Comput. Phys.* 173, 322–347, 10.1006/jcph.2001.6879.